Improving the Convergence of Vector Fitting for Equivalent Circuit Extraction From Noisy Frequency Responses

Improving the Convergence of Vector Fitting for Equivalent Circuit Extraction From Noisy Frequency Responses

Stefano Grivet-Talocia, *Member, IEEE,* and Michelangelo Bandinu

***Abstract*—The vector fitting (VF) algorithm has become a common tool in electromagnetic compatibility and signal integrity studies. This algorithm allows the derivation of a rational approximation to the transfer matrix of a given linear structure starting from measured or simulated frequency responses. This paper addresses the convergence properties of a VF when the frequency samples are affected by noise. We show that small amounts of noise can seriously impair or destroy convergence. This is due to the presence of spurious poles that appear during the iterations. To overcome this problem we suggest a simple modification of the basic VF algorithm, based on the identification and removal of the spurious poles. Also, an incremental pole addition and relocation process is proposed in order to provide automatic order estimation even in the presence of significant noise. We denote the resulting algorithm as *vector fitting with adding and skimming* (VF-AS). A thorough validation of the VF-AS algorithm is presented using a Monte Carlo analysis on synthetic noisy frequency responses. The results show excellent convergence and significant improvements with respect to the basic VF iteration scheme. Finally, we apply the new VF-AS algorithm to measured scattering responses of interconnect structures and networks typical of high-speed digital systems.**

***Index Terms*—Circuit extraction, linear macromodeling, noise, rational approximation, vector fitting.**

I. Introduction

ELECTRICAL interconnects are often responsible for the most relevant deviation of an electronic system from its ideal and desired behavior. This is due to several nonideal effects like crosstalk, spurious couplings, dispersion, losses, radiation, reflections, and other issues that can be found at various integration levels, from chip to package, from board to system, and even in interconnected systems [1]. A thorough electromagnetic compatibility (EMC) and Signal Integrity (SI) assessment of a complete system is a very challenging task due to the extreme complexity of state-of-the-art high-speed applications.

A common approach to handle these difficulties is to view the entire system as a collection of separate and well-defined blocks interacting with each other only through their electrical ports. For example, we can refer to a critical net carrying a sensitive signal from a driver to a receiver through several segments of dispersive transmission lines, interspersed by discontinuities like vias, connectors, and transitions. Each conceptual block in this chain can be characterized separately via direct measurement (if possible) or electromagnetic simulation, in order to derive its input–output port behavior, typically frequency-dependent scattering parameters referred to a common 50 Ω impedance. Once this characterization is available, the common practice is to use some macromodeling tool that is able to provide a rational approximation (in the Laplace domain) of the frequency-dependent transfer matrix of the structure. Since rational approximations correspond in time domain to systems of ordinary differential equations (ODEs), or equivalently, to lumped circuit equivalents [2], [3], the obtained macromodel can be used as a library block into common circuit solvers (e.g., SPICE), in order to carry out a detailed system-level EMC and SI analysis, including signal degradation effects. One of the most critical steps in this modeling strategy is actually the macromodeling tool and the way the rational approximation is computed.

Since its first introduction [4], the algorithm denoted as Vector Fitting (VF) has become a popular tool for macromodel generation starting from measured or simulated frequency-domain responses [5]–[8]. Some application examples ranging from electromagnetic transient analysis to transmission line and interconnect modeling, and even semianalytical evaluation of Green's functions, can be found in [9]–[26]. The main reason for this success is the smart formulation of the rational approximation process, which is cast in terms of an iterative sequence of steps, each corresponding to the solution of simple well-conditioned linear systems [5]–[7]. This formulation provides much better numerical stability and robustness with respect to various alternative and more classical rational approximation schemes (see [28]–[33] for a far from exhaustive list). The VF iterations start with a guess (which can even be randomly selected) on the dominant poles of the structure. This guess is refined through the iterations in a process called *pole relocation*. A brief outline of the VF scheme is recalled in Section II-A for reference.

This study addresses the behavior of VF algorithm in presence of noise in the original frequency responses that characterize the structure under investigation. This issue is relevant every time the responses come from direct measurement, a quite common scenario. Although it is widely recognized that the convergence properties of VF are excellent, and that in very few iterations convergence of the poles is usually achieved, we show that even a small amount of noise can seriously impair or even destroy convergence. The several numerical tests that we performed illustrate how some spurious poles may be "locked" in a wrong

Manuscript received January 25, 2005; revised October 20, 2005. This work was supported in part by the Italian Ministry of University (MIUR) under a Program for the Development of Research of National Interest (PRIN Grant 2004093025).

The authors are with the Department of Electronics, Politecnico di Torino, 10129 Torino, Italy (e-mail: grivet@polito.it).

Digital Object Identifier 10.1109/TEMC.2006.870814

location due to the noise. Section II-B is devoted to an illustration of this problem.

Fortunately, the solution to this no-convergence issue is quite simple. As discussed in Section III, a simple test on the various poles–residues terms at each VF iteration is able to discriminate the spurious poles from the other ones. Then, a hard relocation can be forced so that significant speedup in the convergence is obtained, with a guarantee that no spurious poles are present at the end of the iterations. We denote this process as pole *skimming*. In addition, an *adding* process is devised to increase iteratively the order of the approximation via a guided placement of new poles. This placement is performed by considering the frequency-dependent approximation error through the iterations. The complete algorithm, denoted as *Vector Fitting with Adding and Skimming* (VF-AS) is presented in Section IV. The VF-AS algorithm results stable and converging even in presence of large noise amounts. It avoids use of data conditioning techniques [27] for the suppression of noise before the actual fitting stage. Moreover, it provides automatic order estimation capabilities due to the adding process, once a given accuracy threshold is selected. Several numerical tests presented in Section V illustrate and validate the algorithm.

II. Background and Problem Statement

We recall in Section II-A the basic VF algorithm [4] in order to provide the background material for the further developments and to set the notations. Then, in Section II-B, we illustrate via simple numerical tests the difficulties arising in analyzing noisy frequency responses. These tests will provide the main motivation for this work and will lead to the developments of Section III.

A. The Basic Vector Fitting Algorithm

For simplicity, we refer to a one-port structure characterized by its transfer function $H(s)$ to be approximated by a rational function

$$H(s) \simeq H_\infty + \sum_{n=1}^{N} \frac{r_n}{s - p_n} \tag{1}$$

with unknown poles $\{p_n\}$ and residues $\{r_n\}$. The approximation (1) is to be computed starting from a set of frequency samples $\{H(j\omega_k), k = 1, \ldots, K\}$.

Standard VF is an iterative algorithm that refines an initial estimate $\{q_n^0\}$ of the N dominant poles of the structure. A good practice for the selection of the initial poles is to have them span uniformly the bandwidth under consideration, with poles close to the imaginary axis to avoid ill-conditioning [5]. Let us denote the set of poles that is obtained at the ith iteration as $\{q_n^i\}$, and define the following weight function:

$$\sigma^i(s) = 1 + \sum_{n=1}^{N} \frac{k_n^i}{s - q_n^i} = \frac{\prod_{n=1}^{N} (s - z_n^i)}{\prod_{n=1}^{N} (s - q_n^i)} \tag{2}$$

with unknown residues $\{k_n^i\}$. Then, the following condition

$$\sigma^i(s) H(s) \simeq c_\infty^i + \sum_{n=1}^{N} \frac{c_n^i}{s - q_n^i}, \quad s = j\omega_k \tag{3}$$

is enforced in least-squares sense using the available data $H(j\omega_k)$. The solution of the linear system (3) provides the residues $\{k_n^i\}$ of $\sigma^i(s)$ as well as the coefficients $\{c_n^i\}$ and c_∞^i, which are discarded. Note that (3) implies that the poles of the best rational approximation to $H(s)$ must cancel with the zeros $\{z_n^i\}$ of the weight function. These zeros are easily computed from $\{k_n^i\}$ by solving a simple eigenvalue problem [4], and provide an improved poles estimate that can be used for next iteration, i.e.,

$$q_n^{i+1} = z_n^i, \qquad n = 1, \ldots, N. \tag{4}$$

Iterations are stopped when the desired accuracy is reached. In the absence of noise, usually very few iterations (from one to three-four) are necessary, depending on the complexity of the frequency dependence of the responses to be fitted. Although a formal convergence analysis of the VF algorithm is still not available, experience shows that the set of poles converges quickly

$$\{q_n^i\} \to \{p_n\}. \tag{5}$$

Once these poles are known, a second linear least-squares solution to (1) provides the residues $\{r_n\}$. The rational approximation in (1) is therefore computed using a multistage linear least-squares solution, thus avoiding the use of possibly critical nonlinear optimization techniques. Extensions of the algorithm to the multiport case is straightforward and several implementations are possible [6], [16], [19]. Also available are VF formulations that make use of only time-domain responses [14], [17], such as those obtained by transient full-wave simulation via finite difference techniques (see, e.g., [18]).

A final remark about passivity: Passivity is a fundamental feature that must be ensured, in order to guarantee that a time-domain simulation employing the macromodel remains stable and bounded. In fact, exponential instability may occur during a transient analysis due to even small passivity violations in any of the macromodels forming the network. It is clear that there is no explicit guarantee that the rational approximation computed via VF is passive. However, much attention has been devoted to the problem in the recent literature, and any of the methods in [34]–[38] can be used to enforce the passivity once (at least) the poles of the macromodel are known.

B. Convergence in the Presence of Noise

The simple numerical tests presented in this section illustrate that the good convergence properties of the basic VF algorithm can be significantly deteriorated by noise in the raw data. To illustrate this effect, a set of synthetic rational transfer matrices were generated with varying dynamic order N and port count P. The general procedure for this synthesis is presented in Section V-A, where an extensive Monte Carlo analysis of the various fitting algorithms discussed in this paper is applied to an exhaustive set of test cases. Herein, we consider a single example of transfer matrix with $N = 18$ poles and $p = 2$ ports,

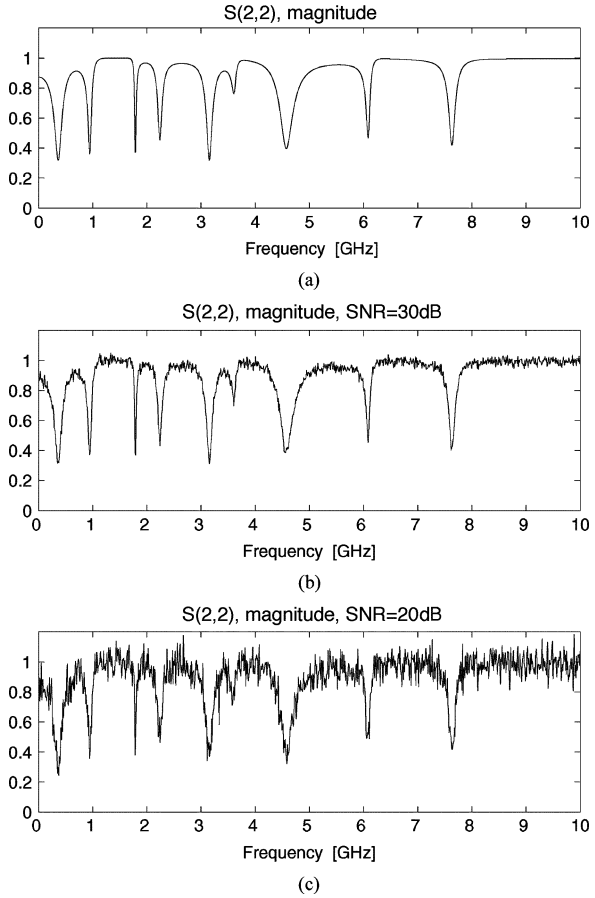

Fig. 1. Two realizations of noisy scattering responses. The magnitude of S_{22} is reported for (b) $\mathrm{SNR} = 30$ dB and (c) $\mathrm{SNR} = 20$ dB. The clean response before noise addition is depicted in (a).

noting that similar results were obtained for the other tests we performed. Scattering representation is considered since this is the most common form in which data are obtained from measurements on real interconnect structures. The synthetic transfer matrix is therefore denoted as

$$\boldsymbol{S}(s) = \boldsymbol{S}_\infty + \sum_{n=1}^{N} \frac{\boldsymbol{R}_n}{s - p_n}. \tag{6}$$

A set of $K = 1000$ frequency samples were computed, spanning a frequency band B encompassing all the poles $\{p_n\}$. We remark that standard VF can be applied directly to identify the set of poles and residues from these frequency samples. These are the ideal conditions for the application of VF, which actually converged in two iterations, producing estimates for poles and residues identical to the "true" ones within machine precision.

New sets of frequency responses were then generated by adding noise to the original responses

$$\hat{\boldsymbol{S}}(j\omega) = \boldsymbol{S}(j\omega) + \boldsymbol{N}(j\omega) \tag{7}$$

where $\boldsymbol{N}$ represents a zero-mean complex-valued and uncorrelated Gaussian noise. Two different SNRs were considered (see the Appendix for details), namely 30 and 20 dB, respectively. Sample realizations of the scattering element S_{22} relative to the two cases are plotted in Fig. 1.

Basic VF algorithm was applied to recover estimates of the N poles and residues matrices in (6) starting from these noisy frequency responses. Denoting the transfer matrices of the macromodels as $\boldsymbol{S}^{\mathrm{fit}}(j\omega)$, the corresponding approximation error can be defined as

$$\hat{\varepsilon} = \|\boldsymbol{S}^{\mathrm{fit}}(j\omega) - \hat{\boldsymbol{S}}(j\omega)\| = \max_{i,j} \|\Delta_{ij}(\omega)\| \tag{8}$$

where

$$\Delta_{ij}(\omega) = \left| S_{ij}^{\mathrm{fit}}(j\omega) - \hat{S}_{ij}(j\omega) \right| \tag{9}$$

represents the frequency-dependent model deviation for the (i, j) matrix entry, and where the rms (energy) norm is used

$$\|\Delta_{ij}(\omega)\| = \left(\frac{1}{B} \int_0^B |\Delta_{ij}(j\omega)|^2 \, d\omega \right)^{1/2} \tag{10}$$

for any scalar function of frequency. Since the "raw" dataset $\hat{\boldsymbol{S}}(j\omega)$ is affected by noise, it is not possible to achieve convergence down to arbitrary precision. The noise variance determines an upper bound on the achievable accuracy of the fit. More precisely

$$\min\{\hat{\varepsilon}\} \simeq \|\boldsymbol{N}(j\omega)\| = \hat{\varepsilon}_{\mathrm{opt}} \tag{11}$$

where the minimum is taken among all possible macromodels (with the same number of poles N) that can be obtained. We denote the quantity $\hat{\varepsilon}_{\mathrm{opt}}$ as *target accuracy* in the following.

The results of the numerical tests were disappointing, since the good convergence properties of VF were not observed with the noisy data. The target accuracy was reached in some cases after many iterations, as in Fig. 2(a). In other cases, for worse noise conditions, no convergence was observed at all [Fig. 2(b)]. These results indicate that VF stagnates in some kind of local minimum during the search of the optimal fit through the iterations. Moreover, for moderate noise levels, which are more common in practical situations, the decrease in the fitting error occurs abruptly, as illustrated in Fig. 2(a), with a possibly large number of iterations required before a significant accuracy improvement is observed.

III. Improving Convergence Via Poles Skimming

The reason for the high sensitivity of the basic VF algorithm to noise is easily understood by considering the evolution of the poles through the iterations. These poles are plotted in Fig. 3 for the test case of Fig. 1(a), i.e., the case with $\mathrm{SNR} = 30$ dB. Two iterations were chosen, namely iterations 30 and 100, corresponding to the "flat" areas in the error plots of Fig. 2(a). The figure shows how reasonable estimates for most of the poles are obtained. However, few poles are still not fitted, and few poles of the rational approximation are stuck in an area of the complex plane that has nothing to do with the target dataset. We denote these as *spurious poles*. These spurious poles are actually responsible for spoiling the convergence. It can be easily seen that these poles are stuck in their location because they try to fit the noise instead of the true data. Equivalently, it can be stated that the VF condition (3), which is the only constraint leading to poles relocation in the basic VF algorithm, is not

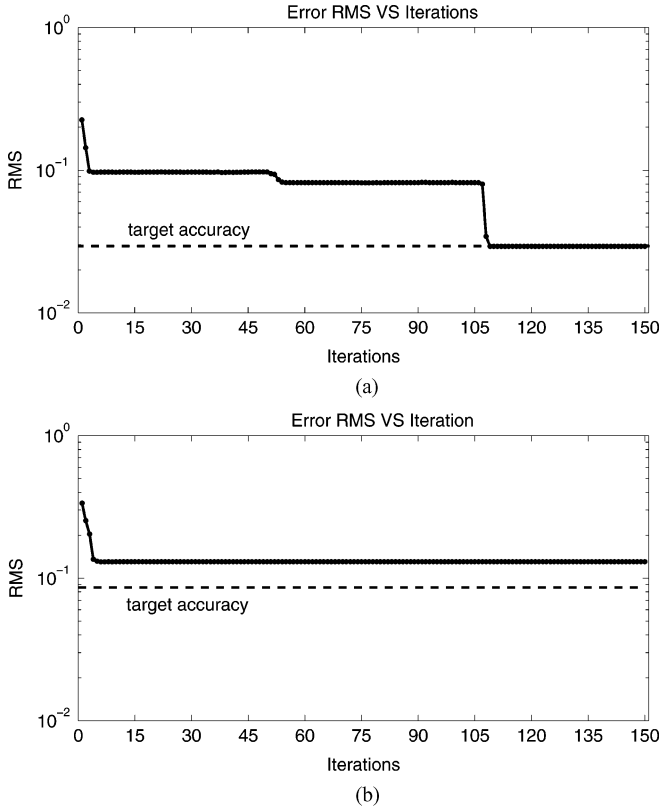

Fig. 2. Convergence problems of a standard VF algorithm in the presence of noise. The plots report the evolution of the approximation error $\hat{\varepsilon}$ during the iterations. Plots (a) and (b) refer to the corresponding plots in Fig. 1, with $\mathrm{SNR} = 30$ and 20 dB, respectively.

strong enough to force the spurious poles to converge to their expected location.

The above considerations lead to the conclusion that a significant enhancement in the convergence could be provided by some "hard" relocation of the poles. This process should be able to automatically detect the spurious poles and to place them in a location of the complex plane that is closer to the true poles. Since any iterative scheme for the solution of a nonlinear problem (such as rational function fitting) is sensitive to the initial guess of the solution, it is expected that a better guess for the poles will also improve the behavior of VF in the presence of noise. The following sections focus on these two complementary aspects. First, we present in Section III-A a possible strategy for the automatic discrimination of the spurious poles. Then, in Section III-B we give a quantitative criterion for the automatic selection of the best location in the complex plane where to relocate the detected spurious poles before continuing with VF iterations.

A. Detection of Spurious Poles

Let us first consider a single pair of complex conjugate poles $\{p_n, p_n^*\}$ and residues $\{r_n, r_n^*\}$ from the partial fraction expansion (1). The associated resonance curve is

$$H_n(j\omega) = \frac{r_n}{j\omega - p_n} + \frac{r_n^*}{j\omega - p_n^*}. \tag{12}$$

We define a band-limited norm as

$$\mu_n^{(p)} = \left(\int_{\Omega_n} |H_n(j\omega)|^p \, d\omega \right)^{1/p}. \tag{13}$$

The integral is over a bandwidth Ω_n defined by the -10 dB level of the resonance curve. Note that this bandwidth is always limited by an upper frequency since $|H_n(j\omega)|$ decays as 20 dB per decade at high frequencies. The actual implementation of (13) uses a summation of samples instead of a continuous integral and differs from (13) only by a constant factor that is equal for all poles. The parameter p is the standard summation index for the mathematical definition of norms in Banach spaces. This parameter can be chosen to tune the relative contributions of magnitude versus frequency spread of the resonance curve. A standard choice is $p = 2$, which denotes the energy (Euclidean) norm. Larger values of p put more weight on the magnitude, up to the limit case $p = \infty$, for which $\mu_n^{(\infty)}$ returns the actual maximum value of the resonance curve. Conversely, smaller values of p, e.g., $p = 1$, put more weight on the frequency spread of the resonance curve. Note that the same norm definition (13) can be employed for the investigation of real poles. However, in all the examples that were processed (both synthetic data or measured data on real structures) we did not find any case where spurious real poles were present. For this reason, we apply only the hard relocation process to complex poles.

The band-limited norms (13) for $p = 1, 2, \infty$ associated to each pole/residue term for the synthetic test case of Fig. 1(a) before noise addition are given in Table I. Tables II and III present the same quantities for the model identified by VF from the noisy dataset at iterations 30 and 100, respectively. The spurious poles already evidenced in Fig. 3 are placed in the last rows of each table. These tables show that the spurious poles are characterized by small values of $\mu_n^{(p)}$, compared to the values associated to the other poles. Actually, a small value of $\mu_n^{(p)}$ relative to the other poles indicates that the nth pair contributes by a small amount to the approximation. It is therefore likely that removing this pair will have a little effect on the accuracy. This is demonstrated in Fig. 4. Fig. 4(a) and (c) presents a comparison between noisy data and VF-generated model (at iteration 30), inclusive of the spurious poles. Fig. 4(b) and (d) shows the same comparison between data and model with the spurious poles removed. There is no visible difference. This confirms that spurious poles have basically a negligible effect on the macromodel accuracy, but they do have a dramatic impact on the convergence properties of VF iterations.

The actual criterion that we chose after extensive testing for the definition of the spurious poles is

$$\frac{\mu_n^{(p)}}{\langle \mu^{(p)} \rangle} < \gamma \ll 1 \tag{14}$$

where $\langle \mu^{(p)} \rangle$ represents the average among all single norms associated to each pole/residue pair and γ is a suitable threshold that controls how sensitive should be the detection of spurious poles. Typical convenient values range from $\gamma = 0.01$ to $\gamma = 0.05$, as confirmed by the values reported in Tables II and III. In all simulations that are presented in this work we used a

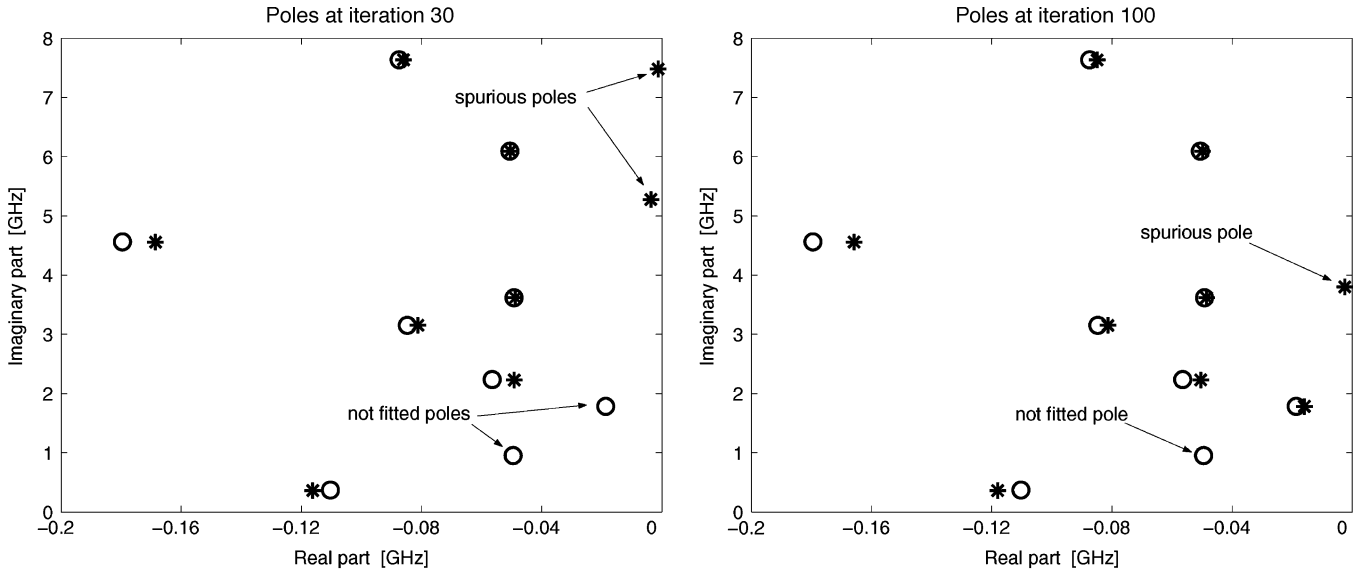

Fig. 3. Spurious poles affecting the convergence for the test case reported in Fig. 1(a). Poles of the original rational function are depicted by circles. Poles at indicated iteration counts are depicted by stars.

TABLE I
POLES p_n, RESIDUES r_n, AND ASSOCIATED NORMS $\mu_n^{(p)}$ FOR THE SYNTHETIC RATIONAL FUNCTION $H(j\omega)$ OF FIG. 1(a)

$p_n/2\pi$ (GHz)	$r_n/2\pi$ ($\times 10^{-1}$ GHz)	$p=1$	$p=2$	$p=\infty$
$-0.1103+j0.3692$	$-1.4737-j0.1360$	90.5117	7.7623	1.3611
$-0.0495+j0.9528$	$-0.3230-j0.0233$	19.3595	2.4894	0.6513
$-0.0187+j1.7845$	$-0.1324-j0.0239$	8.0894	1.6841	0.7099
$-0.0565+j2.2357$	$-0.3075-j0.0218$	18.3918	2.2199	0.5435
$-0.0847+j3.1520$	$-1.1457+j0.0923$	68.9888	6.7866	1.3600
$-0.0492+j3.6175$	$-0.8697-j0.1842$	53.0498	6.8501	1.7945
$-0.1796+j4.5614$	$-1.0542-j0.3623$	65.9053	4.4575	0.6137
$-0.0506+j6.0930$	$-0.7406-j0.0663$	44.4910	5.6619	1.4656
$-0.0875+j7.6349$	$-1.2151-j0.2600$	74.1672	7.1867	1.4172

TABLE II
POLES p_n, RESIDUES r_n, AND ASSOCIATED NORMS $\mu_n^{(p)}$ FOR THE RATIONAL MACROMODEL OBTAINED BY VF AT ITERATION 30

$p_n/2\pi$ (GHz)	$r_n/2\pi$ ($\times 10^{-1}$ GHz)	$p=1$	$p=2$	$p=\infty$
$-0.1162+j0.3616$	$-1.5134-j0.2956$	91.1759	7.6655	1.3117
$-0.0491+j2.2278$	$-0.2648+j0.0108$	15.8834	2.0517	0.5381
$-0.0812+j3.1551$	$-1.0799+j0.1564$	65.4686	6.5909	1.3488
$-0.0488+j3.6188$	$-0.8697-j0.1422$	52.7601	6.8243	1.7934
$-0.1686+j4.5557$	$-0.9993-j0.2905$	61.6516	4.3044	0.6115
$-0.0505+j6.0944$	$-0.7328-j0.0385$	43.9626	5.5977	1.4526
$-0.0860+j7.6355$	$-1.1965-j0.2355$	72.7871	7.1138	1.4150
$-0.0037+j5.2767$	$-0.0011+j0.0026$	0.1782	0.0845	0.0712
$-0.0013+j7.4811$	$-0.0003-j0.0002$	0.0247	0.0117	0.0095

The two spurious poles (see Fig. 3) correspond to the last two rows of the table.

TABLE III
POLES p_n, RESIDUES r_n, AND ASSOCIATED NORMS $\mu_n^{(p)}$ FOR THE RATIONAL MACROMODEL OBTAINED BY VF AT ITERATION 100

$p_n/2\pi$ (GHz)	$r_n/2\pi$ ($\times 10^{-1}$ GHz)	$p=1$	$p=2$	$p=\infty$
$-0.1181+j0.3623$	$-1.5328-j0.2839$	92.5518	7.7159	1.3098
$-0.0159+j1.7840$	$-0.1143-j0.0177$	6.9327	1.5694	0.7177
$-0.0505+j2.2307$	$-0.2712-j0.0106$	16.2041	2.0694	0.5373
$-0.0813+j3.1530$	$-1.0908+j0.1195$	65.7350	6.6149	1.3532
$-0.0485+j3.6195$	$-0.8628-j0.1463$	52.3179	6.7960	1.7937
$-0.1658+j4.5585$	$-0.9879-j0.3059$	61.2700	4.3110	0.6174
$-0.0498+j6.0939$	$-0.7400-j0.0403$	44.2898	5.6875	1.4849
$-0.0850+j7.6353$	$-1.1829-j0.2426$	72.0766	7.0865	1.4180
$-0.0025+j3.8018$	$0.0001+j0.0008$	0.0535	0.0292	0.0259

Only one spurious pole (last row) is present.

summation index $p=2$, but the same results were also obtained with $p=1$. Instead, the norm with $p=\infty$ may be misleading. This is proportional to the magnitude of each residue term $|r_n|$, which is not sufficient for the discrimination of spurious poles for large noise amounts. In fact, the spread of the resonance curve is very important and should be taken into account by using a finite value for p. We denote the application of (14) to detect and remove spurious poles from the model as skimming process.

A few remarks on possible alternative skimming strategies: First, it is possible to define the norms $\mu_n^{(p)}$ in (13) by integrating each resonance curve over the entire modeling bandwidth B, instead of taking only the -10 dB bandwidth Ω_n. We tested this strategy and we got very similar results. However, since integration over the full bandwidth B requires larger computing time, we prefer using the band-limited definition (13). A second alternative skimming strategy would be to compute, for each pole/residue pair, the approximation error of the macromodel with this pair removed. The pair would be labeled as spurious when this approximation error does not change with respect to the error of the complete model with all poles. Note that this definition corresponds to the process that led to the results depicted in Fig. 4. However, this second definition requires larger computing times and was therefore discarded in favor of (13).

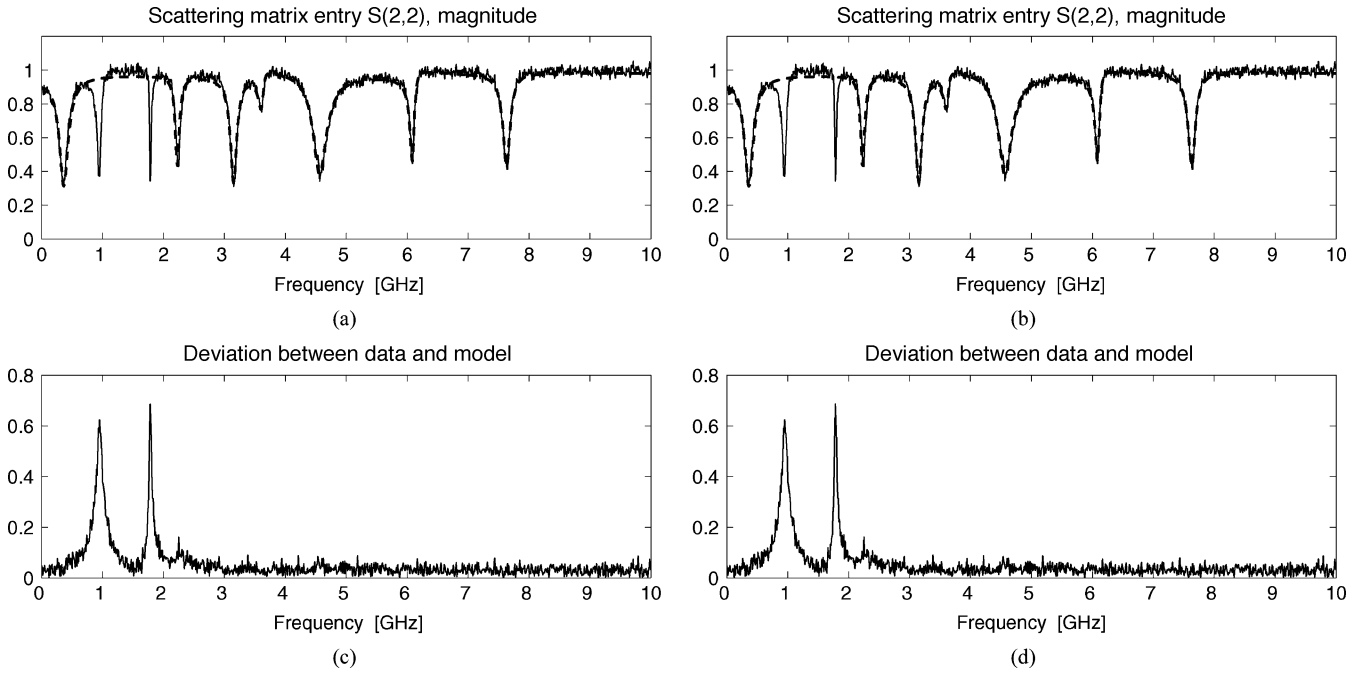

Fig. 4. Plots (a) and (b) show a comparison between data (continuous thin line) and model (thick dashed line) at VF iteration 30. In plot (a) the model includes all poles, whereas in plot (b) spurious poles have been removed. Plots (c) and (d) show the frequency-dependent deviation between data and the corresponding models shown in plots (a) and (b), respectively.

B. Hard Relocation

Fig. 4(c) and (d) shows the frequency-dependent deviation between model and data with and without spurious poles, respectively. From these curves one can easily spot the frequencies at which the approximation is degraded due to missing poles in the model. This is indeed the criterion that we use for the determination of the relocation zones for the detected spurious poles.

With reference to Fig. 4(c) and (d), we compute the local maxima $\omega^n_{\max}$ of the frequency-dependent deviation curves. The number of maxima to be computed equals the number of detected spurious poles. Then, these poles are relocated at

$$p_n^{\text{new}} = (-\text{a} \pm j)\omega^n_{\max} \tag{15}$$

where the real part $a \ll 1$ is chosen so that each new pole is highly resonant (e.g., $a = 0.01$). This is a typical choice for the application of VF [4], since it guarantees good numerical stability of the VF condition (3). We remark that the actual computation of the local maxima $\omega^n_{\max}$ may be tricky in the presence of noise. The actual scheme for the computation of these maxima is presented in Section IV.

There is one additional point to be considered in the suggested hard relocation process. It may happen that the definition of the relocated poles via (15) leads to the placement of a new pole that results close to another pole of the macromodel. This situation should be avoided as much as possible. In fact, the linear system (3) becomes seriously ill-conditioned when two poles are very close because the two columns of the resulting system matrix become almost linearly dependent. This situation is avoided by defining a safety zone, defined as a small neighborhood around each macromodel pole. A new relocated pole will not be allowed to be placed in any of these zones. Several definitions are possible, two of which are depicted in Fig. 5. In Fig. 5(a) the magnitude of each macromodel pole is projected onto the imaginary axis and the result is extended on the left and right by a small amount ν. Thus, each pole leads to a forbidden bandwidth

$$\Theta_n = [|p_n| - \nu, |p_n| + \nu]. \tag{16}$$

If some $\omega^n_{\max}$ falls into any Θ_n, it is redefined at the closest edge of the corresponding forbidden bandwidth. The second definition, illustrated in Fig. 5(b), uses a small circular neighborhood of radius ν in the complex plane around each macromodel pole

$$\hat{\Theta}_n = \{s : |s - p_n| < \nu\}. \tag{17}$$

Also in this case, if some relocated pole p_n^{new} falls into any $\hat{\Theta}_n$, it is redefined at the closest point on the boundary of the corresponding circle. Note (see Fig. 5) that the set of forbidden zones also includes in both cases a small bandwidth around the origin of the complex plane. This additional constraint avoids the presence of very large entries in the linear system arising from (3), having no impact on accuracy and convergence.

Very similar results were obtained using both (16) and (17). The actual criterion that is employed in this work is (16) because to its simplicity of implementation. The complete hard relocation algorithm is detailed in Section IV.

IV. Vector Fitting With Adding and Skimming

The hard relocation process presented in Section III-B is essentially aimed at the determination of a valid guess for the placement of poles before applying the standard VF poles relocation (3). As motivated in the foregoing discussion, this hard relocation is especially needed when noise is affecting the data.

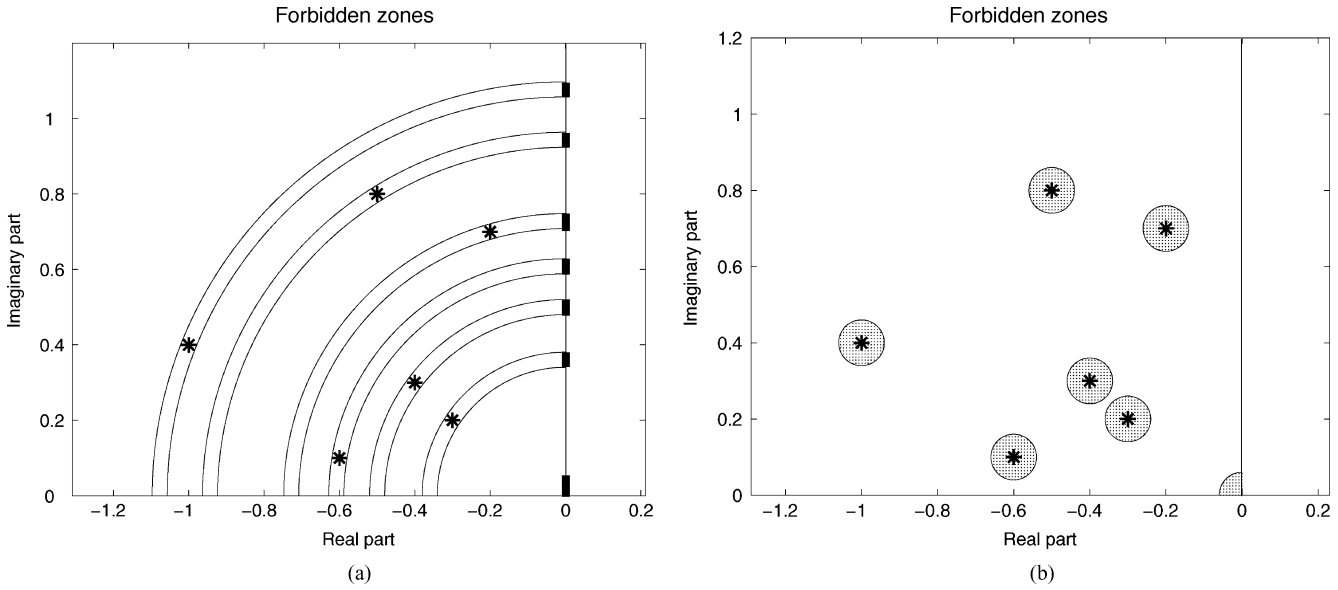

Fig. 5. Two alternative definitions of forbidden zones for the placement of hard relocated poles. Existing (normalized) macromodel poles are depicted by stars.

However, we employ the same strategy to reach a second different objective, related to the automatic order estimation. In fact, the dynamic order (number of poles) to be used in VF must be decided *a priori*. Vector fitting (VF) iterations relocate only the poles to reach minimum approximation error between model and data in least-squares sense. No indication of how many poles are strictly necessary to obtain a prescribed accuracy is available beforehand. Our solution to this problem is a scheme that increases iteratively the number of model poles until sufficient accuracy is obtained. We denote this scheme as adding process. Before describing this iterative process in more detail, we present through an example the general scenario that may occur at a given iteration.

Fig. 6(a) reports a noisy response $\hat{S}_{11}(j\omega)$ of a synthetic two-port rational scattering matrix having 40 poles, with a superimposed Gaussian noise with an SNR of 30 dB. The dashed line is the response of a model having only $N = 30$ poles, obtained via standard VF after four iterations. The difference between model and data is evident, mainly due to the insufficient number of model poles. The frequencies of all the poles of the original transfer matrix are denoted by triangles, with filled triangles indicating those poles that have been reasonably approximated in the model and empty triangles indicating the poles that still need to be identified and approximated. In order to increase the set of model poles, we consider the frequency-dependent error $\Delta_{ij}(\omega)$ of (9) between current model and data reported in Fig. 6(b). The local maxima of this curve are candidates for the placement of both new poles (to increase the model order) and hard-relocated spurious poles. Note that in case frequency-dependent weighting is employed to control the accuracy in selected frequency bands, the modified frequency-dependent error

$$\Delta_{ij}(\omega) = \left| S_{ij}^{\text{fit}}(j\omega) - \hat{S}_{ij}(j\omega) \right| \rho(\omega) \tag{18}$$

should be used instead of (9), where $0 \leq \rho(\omega) \leq 1$ is a suitable weighting function.

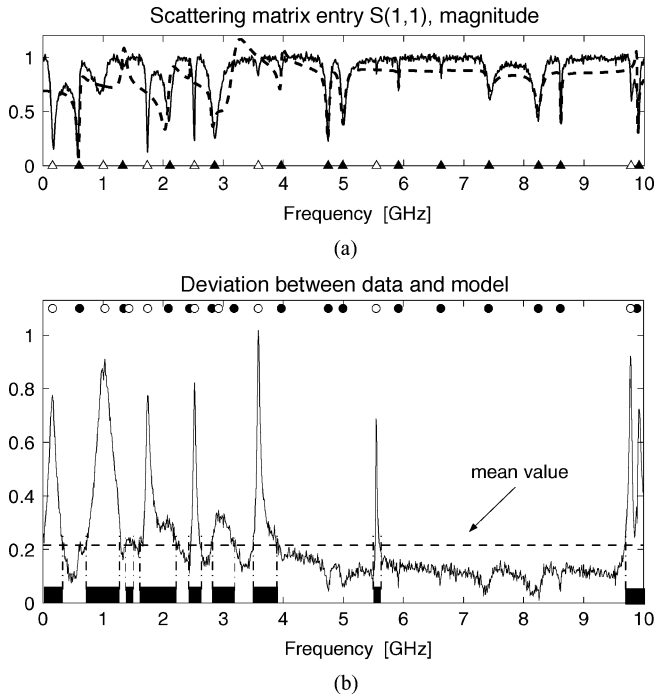

Fig. 6. Characterization of the adding process.

Becuase of the presence of noise, the error indicators $\Delta_{ij}(\omega)$ are also noisy, implying that some smoothing should be applied before the actual computation of the maxima. We deal with this issue using a different approach. First, the mean value over the entire bandwidth B

$$\langle \Delta_{ij} \rangle = \frac{1}{B} \int_B \Delta_{ij}(\omega)\, d\omega \tag{19}$$

is computed [the dashed line in Fig. 6(b)]. Its intersections with the error curve determine a set of separate frequency bands Ψ_n

Algorithm 1 (*Vector Fitting with Adding and Skimming*)

Require: N_{start} (initial number of poles)
Require: $N_{\max}$ (maximum number of poles)
Require: N_{add} (number of poles for the *adding* process)
Require: I_1, I_2, I_3 (starting, intermediate, and final VF iteration count)
Require: γ (threshold for the *skimming* process)
Require: $\hat{\varepsilon}_{\min}$ (stopping accuracy)
Require: α (threshold to detect error stagnation)
1: Apply standard VF with N_{start} poles for I_1 iterations
2: Compute model error $\hat{\varepsilon}$
3: **while** $\{(\hat{\varepsilon} > \hat{\varepsilon}_{\min})$ **and** $(N < N_{\max})$ **and** $(\delta\hat{\varepsilon} > \alpha\hat{\varepsilon})\}$ **do**
4: *Skimming*: determine the number N_{skim} of spurious poles using (14) and remove them
5: Compute error $\Delta(\omega)$ between model and data
6: Compute forbidden bandwidths Θ_n via (16)
7: Compute bandwidths Ψ_n according to (20)
8: *Adding*: insert $N_{\text{add}} + N_{\text{skim}}$ poles using (15)
9: Perform I_2 iterations of standard VF and compute model error $\hat{\varepsilon}$
10: **end while**
11: *Skimming*: check for and remove the remaining spurious poles using (14)
12: Perform I_3 iterations of standard VF

over which all frequency samples of $\Delta_{ij}(\omega)$ exceed $\langle\Delta_{ij}\rangle$

$$\omega \in \Psi_n \quad \Longleftrightarrow \quad \Delta_{ij}(\omega) > \langle\Delta_{ij}\rangle. \tag{20}$$

These bands are highlighted by thick segments in the plot. We allow only one maximum to be searched for each of these frequency bands. Moreover, the bands are ranked according to the peak value of the error curve. Therefore, in case several new poles need to be added to the model, they are automatically associated to the frequency bands characterized by the largest deviations. For this example, a total of 9 separate frequency bands are found, allowing for the insertion of a maximum number of 9 new pole pairs in the model. The corresponding frequencies $\omega_{\max}^n$ are depicted by empty circles in Fig. 6(b), whereas filled circles are the existing poles of the model. It should be noted that the frequencies associated with the largest peaks have a one-to-one correspondence to the poles of the original function that have not yet been identified [empty triangles, Fig. 6(a)]. This gives confidence for the automatization of this pole-placement scheme. Of course, the actual placement of the new poles must take into account the forbidden zones already discussed in Section III-A and expressed by (16). Also, in case of multiple responses to be considered in the fit, a global measure $\Delta(\omega)$ for the frequency-dependent deviation of the model from the data can be defined by taking either the frequency-dependent worst case or some kind of average among all responses.

We now combine the skimming and relocation of spurious poles described in Section III-A with the above described adding process into a single algorithm, denoted as vector fitting with adding and skimming (VF-AS). This algorithm should be considered as an improved version of the standard VF, capable of dealing with noisy frequency data and with automatic order estimation. The main VF-AS steps are outlined in Algorithm 1, together with the parameter set that allows to customize the algorithm to specific needs. First, a standard VF is applied (step 1) using an initial number of poles N_{start}. When no *a priori* information on the structure is available, a small number of initial poles should be chosen, letting the algorithm determine the correct order. Then, the obtained model is checked by testing a suitable stopping condition (step 3: a precise justification for this condition will follow in the next paragraph). If the model is not yet satisfactory, a skimming process is applied (step 4) to detect and remove any spurious poles, which may be expected due to the presence of noise. Then, the various hard-relocation bandwidths Ψ_n and the forbidden bandwidths Θ_n are combined to get the optimal locations for the placement of new poles. The adding process (step 8) inserts N_{add} new poles in addition to the N_{skim} hard-relocated spurious poles. Standard VF iterations are then used (step 9) to relocate the current poles and to minimize the model error. The entire procedure is repeated until the stopping condition is fulfilled. A final skimming process followed by few standard VF iterations is applied to remove any spurious poles that might have been left in the model.

We consider now in more detail the stopping condition in step 3. This condition provides a test for the suitability of the macromodel at current iteration. First, we note that a plain check on accuracy by a stopping threshold $\hat{\varepsilon}_{\min}$ on the approximation error is not sufficient. In fact, this threshold might be easily set by the user to a value that is too small with respect to the (unknown) noise level. With reference to Fig. 2, if $\hat{\varepsilon}_{\min}$ is smaller than the dashed lines (the target accuracy $\hat{\varepsilon}_{\text{opt}}$), the algorithm will never stop since the noise level is too large. Therefore, an additional stopping condition limiting the order to a maximum value $N_{\max}$ is also needed. It is nonetheless clear that this value also requires some expert knowledge of the data from the user.

The above considerations lead to a third additional stopping condition, which results particularly useful when significant noise is present. This condition is aimed at the determination of the minimum achievable error $\hat{\varepsilon}_{\text{opt}}$ by tracking the decay of the approximation error through the adding iterations. The more the poles are added, the smaller the approximation error is expected to be. However, when the number of poles reaches the correct order, no error decay is expected anymore. This is illustrated by Fig. 7, which depicts the behavior of the approximation error $\hat{\varepsilon}$ through the VF-AS iterations, applied to the two test cases of Fig. 1. This leads to the test

$$\delta\hat{\varepsilon} < \alpha\hat{\varepsilon} \tag{21}$$

where $\delta\hat{\varepsilon}$ is the error decay with respect to previous iteration (or with respect to an average among m few previous iterations) and $\alpha \ll 1$ is a suitable threshold. When (21) is fulfilled, the error is approximately constant, and it can be argued that the noise floor has been reached. After several tests we conclude that good values for α are in the range between 0.01–0.05, and with $m = 2$ or 3.

Fig. 7 reports the decay of the approximation error versus iterations for two different VF-AS parameter settings. Fig. 7(a) and (b) uses the most conservative choice (small number of initial poles, small number of poles for the adding process). Fig. 7(c) and (d) uses instead multiple pole addition at each iteration and a larger starting order. This choice results into a much smaller number of iterations to reach the noise floor. Note that

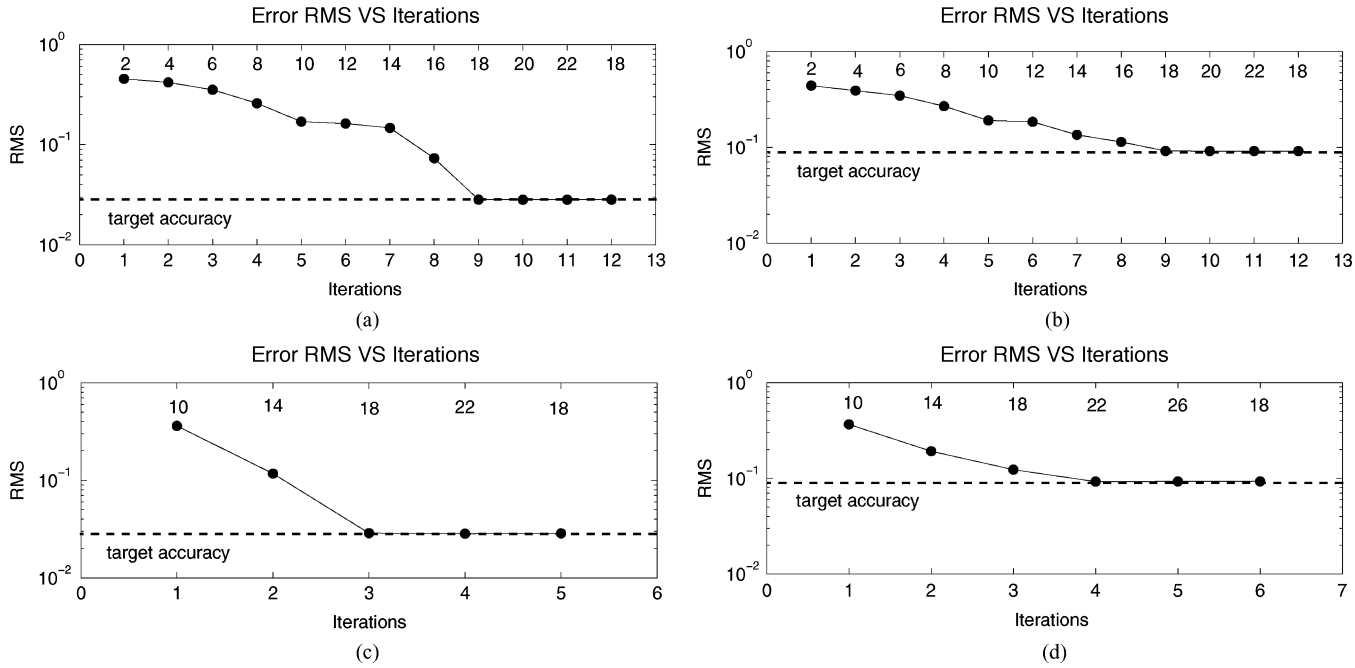

Fig. 7. Error $\hat{\varepsilon}$ versus iterations for the VF-AS algorithm. Plots (a) and (c) refer to the example of Fig. 1(a) with $\mathrm{SNR} = 30$ dB, while plots (b) and (d) refer to Fig. 1(b) with $\mathrm{SNR} = 20$ dB. The only difference between top and bottom plots is on the choice of VF-AS controlling parameters. In particular, top plots (a) and (b) use a conservative choice $N_{\mathrm{start}} = N_{\mathrm{add}} = 2$, whereas bottom plots (c) and (d) use $N_{\mathrm{start}} = 10$ and $N_{\mathrm{add}} = 4$ to reduce the number of VF-AS iterations. The top scale in each plot reports the number of macromodel poles at each iteration.

m iterations beyond the correct order (18) are needed in order to detect the saturation of the error curve. The final skimming in the VF-AS algorithm (corresponding to the last point in all parts of Fig. 7) removes any spurious poles that may have been added during the iterations. These figures should be compared with Fig. 2, reporting the same error plot obtained by standard VF. The advantages of VF-AS are evident. Extensive validation of the VF-AS algorithm as well as numerical results arising from its application to synthetic and real measured data follow in Section V.

V. Numerical Results

We present in this section some numerical results to illustrate the advantages of the new proposed VF-AS algorithm. Section V-A is devoted to an extensive Monte Carlo analysis for a detailed study of the robustness of VF-AS, using parameterized noise levels. Section V-B reports some application examples, namely interconnect structures and networks known via measured scattering responses.

A. Monte Carlo Robustness Study

This section presents an extensive validation of the VF-AS algorithm in order to assess its noise sensitivity and robustness. This kind of study requires a very large number of tests on representative data samples, together with a statistical analysis of the results. It is clear that the use of real measured data is impractical for this purpose, since the number of independent structures and measurements that would be required for a meaningful interpretation would be too large. Therefore, we rely on synthetic data for this robustness study.

We devised an automatic procedure for the synthesis of the scattering matrix of frequency responses for a randomly generated lumped multiport. The generation algorithm, outlined in the Appendix, ensures that the responses represent a passive structure with a predetermined bandwidth and number of poles and ports along with parameterized losses and superimposed noise. As a result, these randomly generated responses are almost undistinguishable from actual measurements of real interconnect structures and therefore representative of real cases for which a macromodel would be needed.

The robustness of VF-AS algorithm to noise was investigated via a Monte Carlo analysis. Since both the synthesis of the noisy rational responses and the VF-AS algorithm are fully automatic, a very large number of numerical tests have been performed for many parameter combinations. In particular, several realizations with order N ranging from 8 up to 50 and loss factor ϑ ranging from 10^{-4} (low-loss) up to 0.5 (high-loss) have been analyzed. We report here only few representative cases, noting that similar results were obtained for all other tests. The testing procedure follows the steps itemized below.

1) Generate a set of "clean" scattering responses $\boldsymbol{S}(j\omega)$ via the procedure outlined in the Appendix.
2) For each of the above, generate a set of independent noisy realizations $\hat{\boldsymbol{S}}(j\omega)$ with a fixed SNR value. A loop over the SNR is performed to test the algorithms under varying noise conditions.

3) Apply the VF-AS algorithm to estimate order, poles, and residues from the noisy responses.
4) Apply the standard VF to the noisy responses to estimate poles and residues, using the correct number of poles to initialize the algorithm; the initial set of poles is chosen following the standard rules for VF, i.e., linearly spaced throughout the modeling bandwidth.
5) Apply the standard VF to the noisy responses by choosing the initial poles coincident with the (known) exact poles of the synthetic scattering responses. This test provides the "ideal" setting for VF, since no pole relocation should occur other than a small adjustment due to the presence of noise. It is expected that no better results under any noise condition can be obtained with any other fitting algorithm.
6) Compute performance metrics and collect the results.

A few remarks on the adopted performance metrics, which differ from the approximation error already introduced in (8). The main definition of the identification error (in decibels) for a fitted model, obtained either via standard VF or VF-AS, is the following:

$$\varepsilon_{ij} = 10 \log_{10} \frac{\|S_{ij}^{\rm fit} - S_{ij}\|^2}{\|S_{ij}\|^2} \tag{22}$$

where $S_{ij}^{\rm fit}$ is the (i,j) matrix entry of the fitted model. All norms are computed as the rms value (10) among all available frequency samples. A single accuracy measure for the entire transfer matrix is then obtained by taking the worst among all entries

$$\varepsilon = \max_{i,j} \{\varepsilon_{ij}\}. \tag{23}$$

Note that these metrics are computed using the clean responses as the reference, since these are explicitly known. Conversely, the approximation error of (8), which is actually used to test convergence during the VF or VF-AS iterations, uses the raw (noisy) dataset as the reference, since this is the only one to be known in practical applications.

Expression (22) can be rewritten in terms of SNR as

$$\varepsilon_{ij} = -{\rm SNR}_{\rm dB} + 10 \log_{10} \frac{\|S_{ij}^{\rm fit} - S_{ij}\|^2}{\|N_{ij}\|^2}. \tag{24}$$

This expression implies that the value $-{\rm SNR}_{\rm dB}$ represents an important threshold for the approximation error. A value of ε_{ij} smaller than this threshold indicates that the model deviation from the clean responses is smaller than the noise variance. This is an indication of small sensitivity of the fitting algorithm with respect to noise. Conversely, an approximation error larger than this threshold indicates significant deterioration in the approximation, since the accuracy degradation is larger than the noise variance. If the error ε_{ij} is plotted versus SNR using a decibel scale, this threshold results in a straight line with slope -1. All subsequent plots will also report this threshold for reference.

Figs. 8 and 9 report the results of the described testing process. The only difference between the two figures is the loss factor ϑ. Both examples refer to structures with $N = 30$ poles and $P = 2$ ports, although only the results for the S_{11} element are reported. In both cases 15 noisy realizations for each of three different clean set of responses were analyzed, for a total number of 45 noisy realizations. This number allows for a meaningful statistical interpretation of the results. Figs. 8(a) and 9(a) show the approximation error plotted versus SNR in the case of standard VF initialized with the exact poles. These plots show that for all tested noise levels, and up to the very large ${\rm SNR} = 10$ dB, the deviation of the model from the clean responses is significantly less (by more than 10 dB) than the SNR value. This indicates that when no pole relocation is needed, due to a good choice of initial poles, the standard VF algorithm has a very small noise sensitivity even for large noise amounts. Figs. 8(b) and 9(b) show the results of the standard VF. Only for SNR values more than 40–50 dB the standard VF is able to reproduce the results of the ideal (exact poles) setting. For higher noise levels, the convergence problems due to the spurious poles significantly affect the accuracy of the results. In particular, several realizations led to an approximation error larger than the SNR threshold. This is a clear indication of sensitivity to noise. Figs. 8(c) and 9(c) show the results of the proposed VF-AS algorithm. These are basically undistinguishable from the results of the ideal (exact poles) VF, for both reported cases and for any noise level. This confirms that the proposed adding and skimming processes are very effective in handling the convergence problems of a standard VF, even in the presence of large amounts of noise. Finally, Figs. 8(d) and 9(d) show the estimates of the model order obtained by the VF-AS. The estimates coincide with the exact number of poles $(N = 30)$ for most realizations with ${\rm SNR} > 20$ dB. For smaller SNR, and especially for the more lossy case $\vartheta = 10^{-2}$ of Fig. 9, the noise is so large that the same (small) approximation error may be achieved by using a reduced number of model poles. This is an indication of automatic (accuracy-controlled) model order reduction capabilities of the proposed VF-AS scheme.

B. Applications

We begin with an application of the VF-AS scheme to the macromodel generation for the structure depicted in Fig.10. This is a simplified geometry, which was investigated to illustrate the effects of lumped and distributed coupling between power/ground conductors and signal conductors on typical Printed Circuit Boards (PCB). Ports 1 and 2 are located between the power and ground conductors., while ports 3–6 provide the termination to a coupled stripline structure. The structure was analyzed using a full-wave transient solver based on the finite integration technique [39]. In this simulation, the PCB was terminated on each side with perfect magnetic walls and the reference impedance for each port was set to the standard value $R_0 = 50\ \Omega$. After the application of fast Fourier transform to the transient data obtained by the field solver, the frequency-dependent 6×6 scattering matrix was obtained up to a maximum frequency of 3 GHz, with a total of $K = 1021$ samples per response.

Some of the scattering responses are depicted by continuous thin lines in Fig. 11. This dataset provides the input to the VF-AS scheme for the macromodel generation. We remark that this structure is quite significative for the assessment

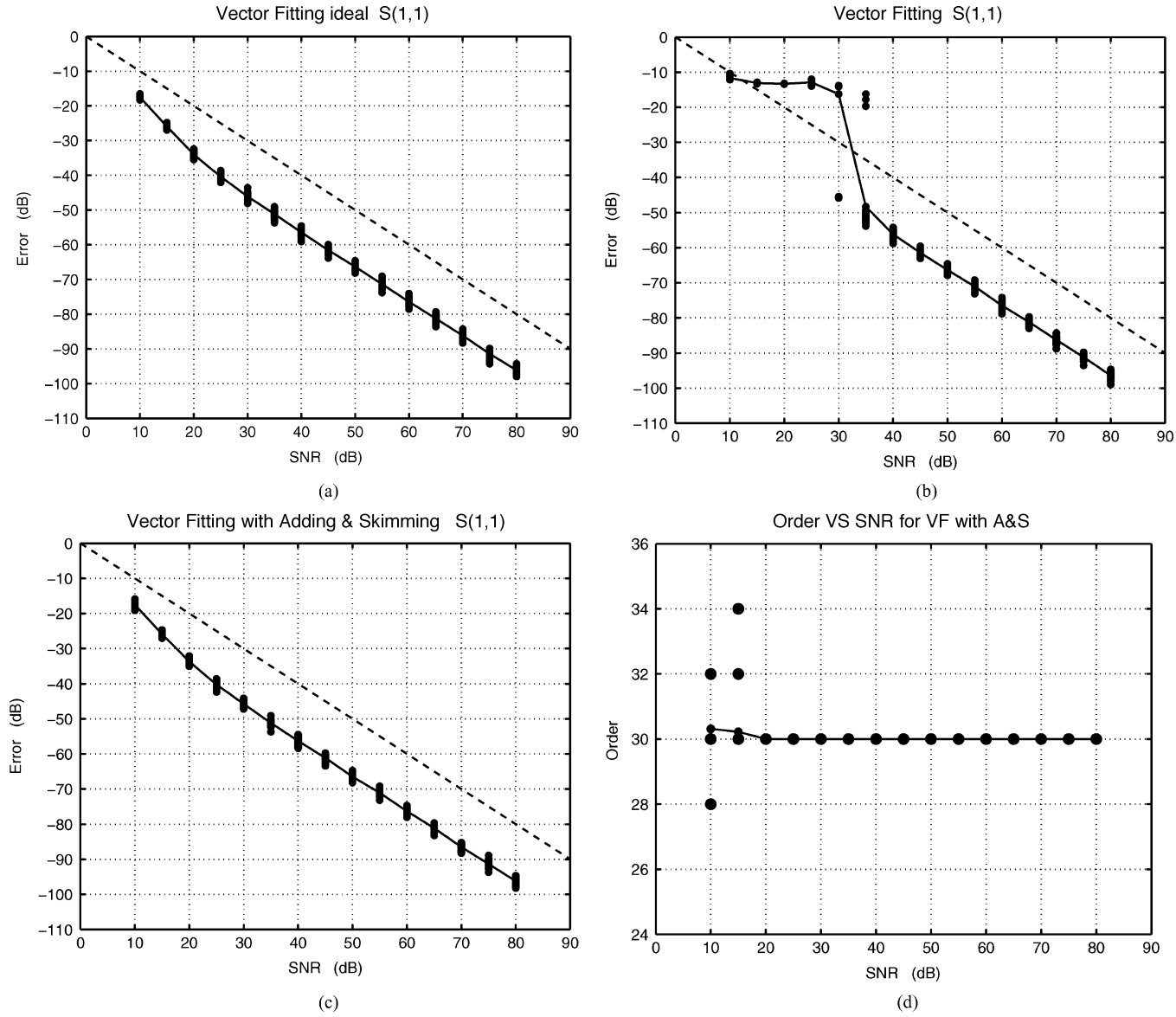

Fig. 8. Noise sensitivity of various VF implementations applied to a 30-pole two-port with normalized loss factor $\vartheta = 10^{-4}$. Plots (a)–(c) report the identification error ε for three different fitting algorithms, namely (a) ideal (exact poles) VF, (b) standard VF, and (c) VF-AS. Plot (d) reports the order estimates obtained by VF-AS. In all the plots, the cloud of dots represents the results obtained for each of 45 different realizations. The continuous lines indicate the average among all realizations.

of a macromodeling tool, since several different physical phenomena contribute to the shape of the frequency responses. On one hand, the resonances of the power/ground planes, clearly visible in $S_{1,1}$ and $S_{1,2}$, are mainly determined by the board size and by the location of the power/ground ports. On the other hand, the responses of the coupled striplines are mainly determined by their cross section and length (see $S_{3,3}$ and $S_{3,4}$ in Fig. 11). However, the power/ground resonances are also visible, to a lesser extent, in the stripline responses. These two sets of resonances are not directly related one to each other and may require different sets of poles in the macromodel. Finally, the distributed coupling between power/ground and signal conductors is highlighted by $S_{1,3}$.

The above description of the physical and geometrical features of the structure in Fig. 10 leads to the conclusion that the number of poles required by an accurate macromodel is difficult to predict based on *a priori* assumptions. An automatic order estimation is required for the determination of the optimal dynamic order once a desired accuracy has been set. The VF-AS is ideally suited for this task. The algorithm was run using $N_{\text{start}} = 60$ initial poles for each column of the transfer matrix and $N_{\text{add}} = 2$ poles for each Adding step. The stopping accuracy was set to $\hat{\varepsilon} = 10^{-3}$, with a threshold for error stagnation $\alpha = 0.1$. Finally, the threshold for the skimming process was set to a small value $\gamma = 0.01$ since thereis no significant noise in the data. The skimming processis activated only when less

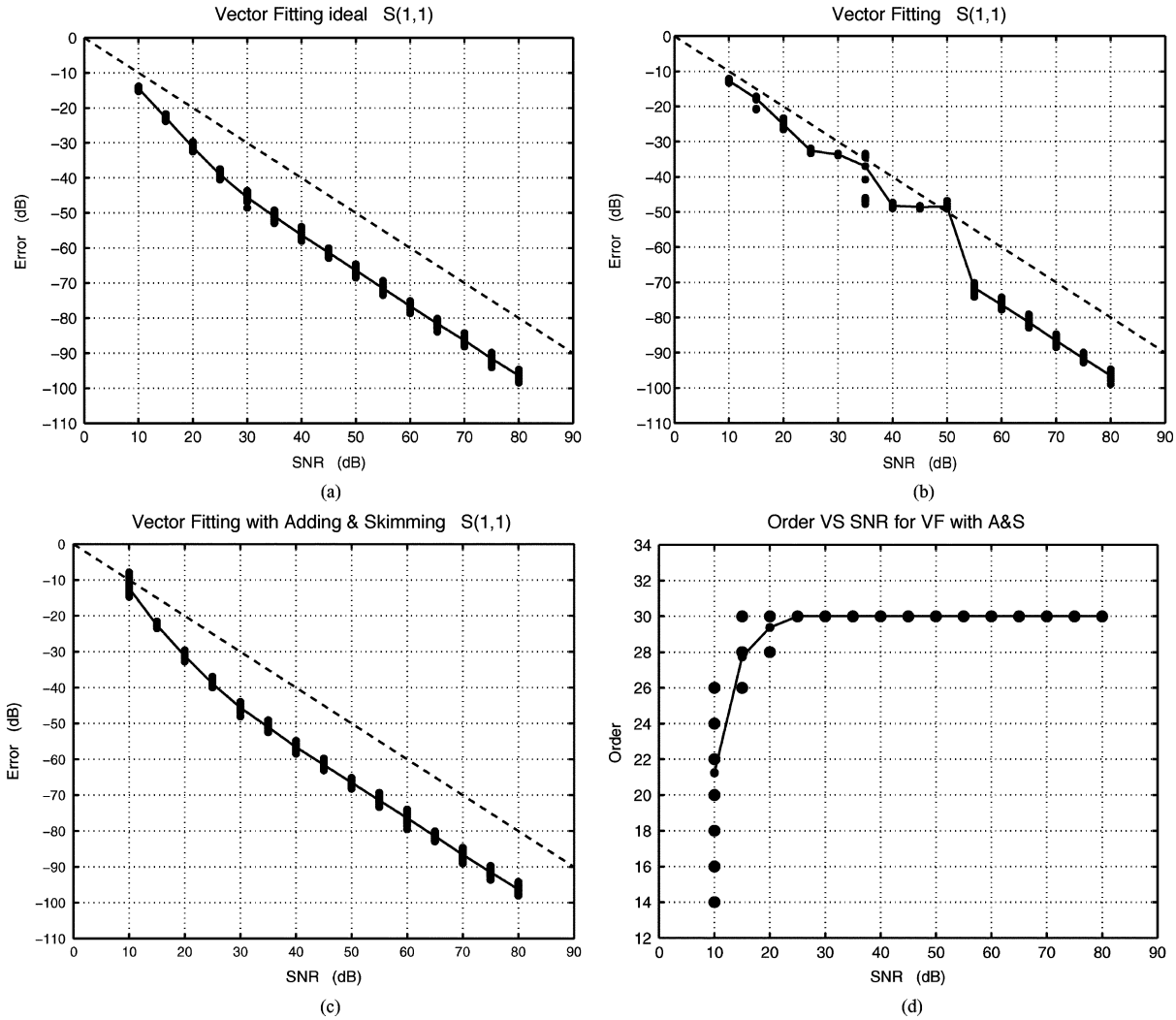

Fig. 9. Noise sensitivity of various VF implementations applied to a 30-pole two-port with normalized loss factor $v = 10^{-2}$. Plots (a)–(c) report the identification error ϵ for three different fitting alogrithms, namely (a) ideal (exact poles) VF, (b) standard VF, and (c) VF-AS. Plot (d) reports the order estimates obtained by VF-AS. In all the plots, the cloud of dots represents the results obtained for each of 45 different realizations. The continuous lines indicate the average among all realizations.

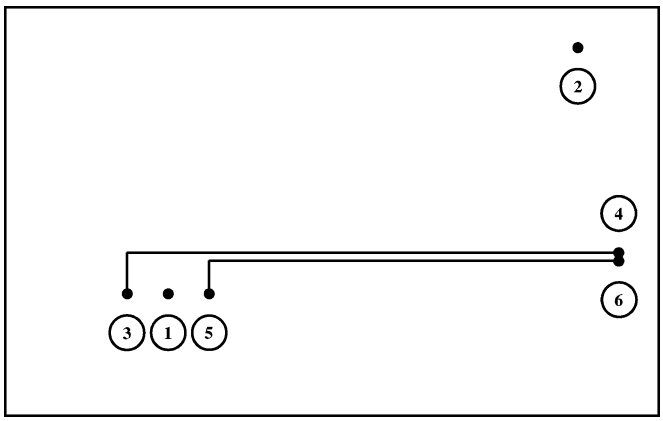

Fig. 10. PCB structure used as a benchmark for the VF-AS scheme. The board size is 16 $\times$10 cm, with a power-signal-ground configuration ($\sigma = 5.8 \times 10^7$ S/m for all conductors). Each layer ($\varepsilon_r = 4.2, \tan\delta = 0.001$) is 0.7 mm high. The stripline conductors are 0.2 mm wide with a separation in the coupled segment of 0.5 mm. Port locations are, in millimeter units from the bottom-left corner, 1:(40, 30), 2:(140, 90), 3:(29, 31), 4:(150, 41.1), 5:(49, 31), and 6:(150, 40.6).

significant poles/residues appear to converge before more important ones. This is indeed the case when the number of poles is smaller than the optimal model order, because the set of poles that will converge depends on the choice of the initial poles.

The results of the VF-AS scheme are plotted in Fig. 11 with dashed lines. All the responses are fitted with excellent accuracy, since there is no visible difference between model and data. The main factor that led to terminate the VF-AS iterations was the stagnation condition (21). The maximum resulting deviation among all responses and all frequency samples was 5.2×10^{-3}, with a maximum number of 78 poles. These figures illustrate the excellent results that can be achieved by VF-AS.

We conclude the set of application examples by presenting two cases of macromodels generated from actual measurements. The first structure is a 2-cm stripline including the discontinuities caused by the signal launches. The second structure is a connector. The frequency-dependent scattering parameters for both structures were obtained via direct Vector Network

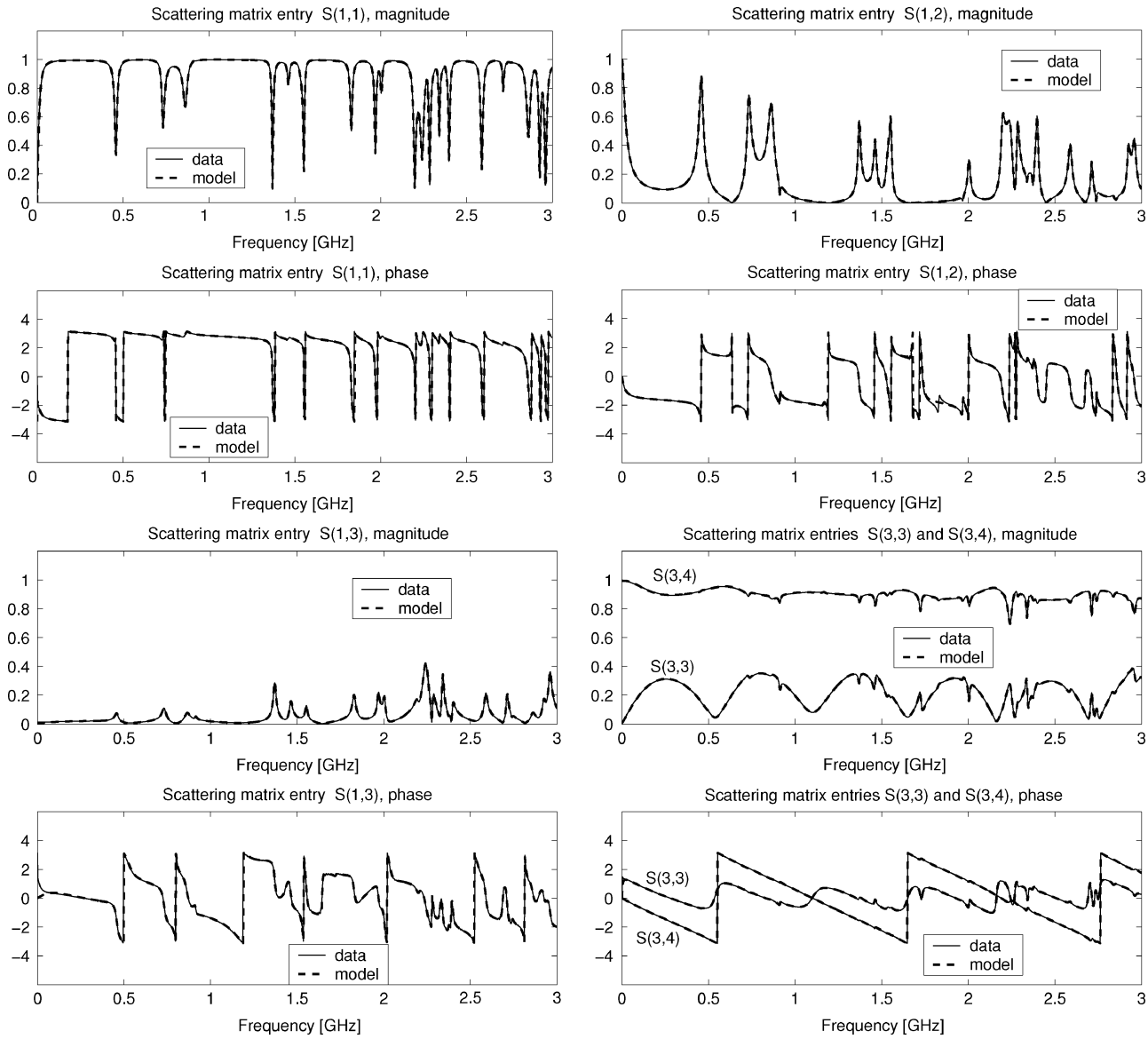

Fig. 11. Selected scattering responses for the structure depicted in Fig. 10.

Analyzer (VNA) measurements (courtesy of IBM) up to a maximum frequency of 40 and 20 GHz, respectively. This extended frequency spectrum is required by an accurate signal integrity characterization for the the high-speed waveforms that are intended to propagate along these interconnects. Some selected responses of the two structures are depicted in Figs. 12 and 13, respectively. Note that although we are unable to show the actual geometries due to a confidentiality agreement, the frequency responses are quite representative for the corresponding classes of interconects, being characterized by some general features, such as propagation delays (visible from the phase variations) and attenuation (visible from the magnitude responses).

The VF-AS algorithm was applied, and a macromodel was obtained for both structures. The relevant control parameters for the skimming and adding processes were set to $\gamma = 0.01, \alpha = 0.1$, and $N_{\rm add} = 2$, with $N_{\rm start} = 50$ for the stripline and $N_{\rm start} = 80$ for the connector. All responses were considered at the same time in the stripline model generation, leading to a macromodel with 66 common poles. The connector model was instead generated by treating independently each column of the scattering matrix, obtaining a maximum number of poles of 116. As for the other examples, also for these cases, the order was automatically determined during the iterations by the error stagnation condition (21).

The two responses characterized by the largest deviation for both models are depicted in Figs. 12 and 13. These plots show that the achieved accuracy is excellent and that the deviation between measurements and models is hardly visible on the adopted scale. Therefore, we also included a plot of the frequency-dependent deviation $\Delta_{i,j}(\omega)$ in both these figures. These plot also reveal the presence of noise in the measurements, thus justifying the use of the more robust VF-AS algorithm for the macromodel generation.

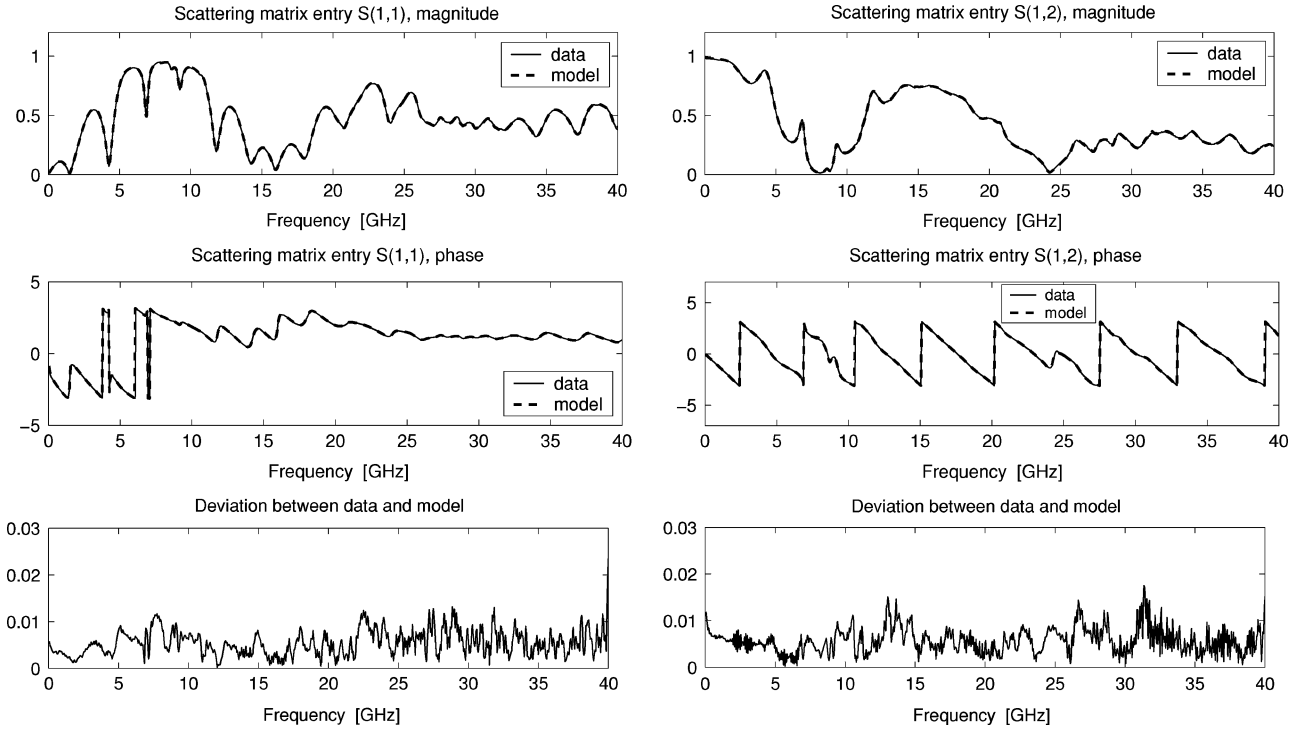

Fig. 12. Selected scattering responses of a 2-cm stripline including launches.

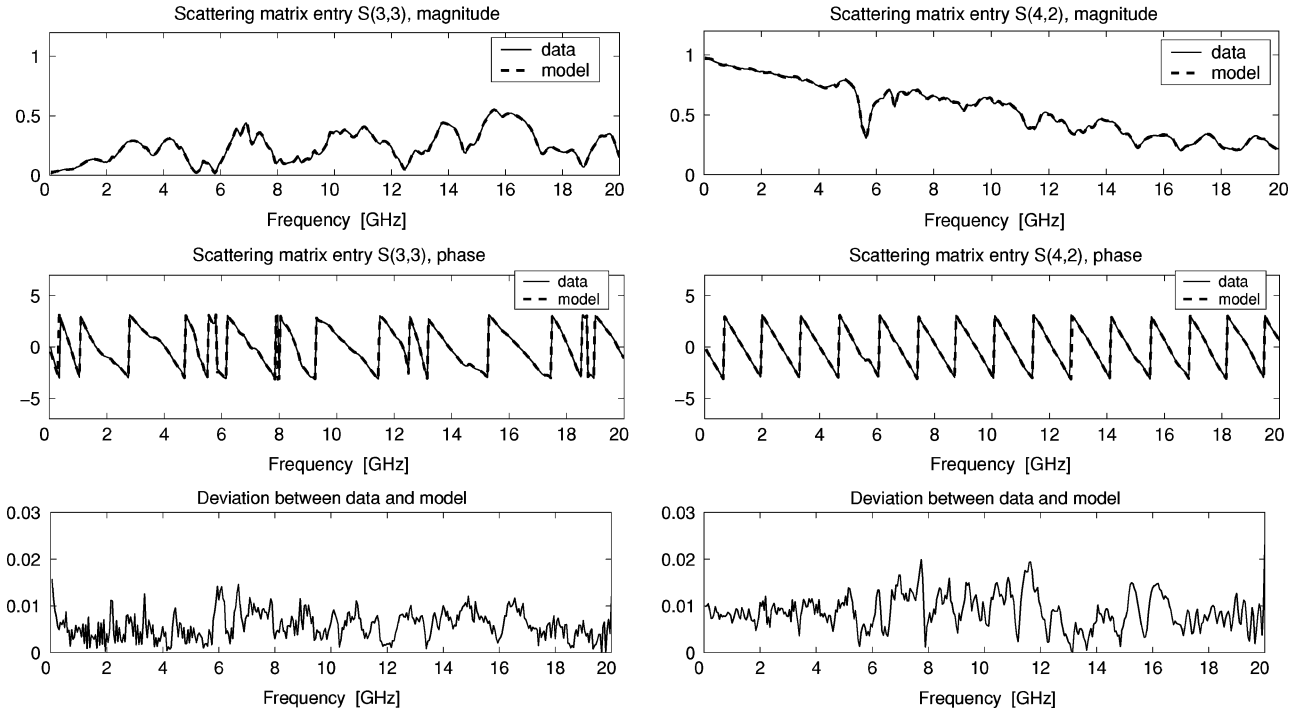

Fig. 13. Selected scattering responses of a connector.

VI. Conclusion

We have presented an improved version of the standard VF poles relocation algorithm for the generation of linear macromodels. The new algorithm, Vector Fitting with Adding and Skimming (VF-AS), is based on the identification of spurious poles and on an incremental poles adding process. The combination of these new features allows the automatic order estimation embedded into an iterative process that results quite robust to noise. The validations provided in this work show that, even with small SNRs, the VF-AS algorithm is highly efficient and reliable. Conversely, application of the standard VF

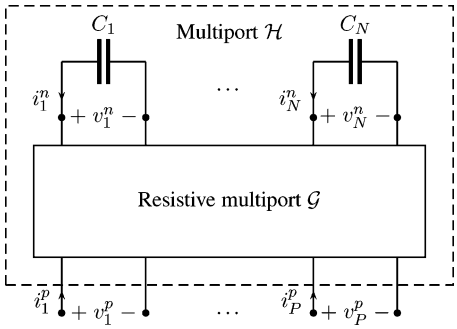

Fig. 14. Structure of synthetic multiport $\mathcal{H}$.

iterations would result in poor or no convergence at all even in the presence of small noise amounts. The application of the new algorithm to some interconnect structures and networks found in high-speed digital systems illustrates the excellent accuracy that can be achieved.

We do not suggest to replace the standard VF algorithm with the one discussed in this paper. However, we have shown a possible solution for handling noisy frequency responses within the framework of the pole relocation strategy typical of the VF iteration. Furthermore, the proposed algorithm can be implemented by minimal modifications to existing VF routines. Finally, we remark that the considerations and the solutions proposed in this paper are mainly empirical and experience based. In fact, a formal convergence analysis of VF remains an open problem that deserves attention in further studies.

APPENDIX

AUTOMATIC GENERATION OF SYNTHETIC NOISY RATIONAL RESPONSES

We now present the adopted synthesis procedure leading to the scattering responses for a randomly generated multiport $\mathcal{H}$. We assume for $\mathcal{H}$ the basic structure depicted in Fig. 14. The multiport has P interface ports with associated port voltages and currents denoted by $(v_i^p, i_i^p), i = 1, \ldots, P$, and collected in arrays $\boldsymbol{v}^p, \boldsymbol{i}^p$. The solid box denotes a purely resistive linear multiport $\mathcal{G}$ having $N + P$ ports, with the additional internal N ports having port voltages and currents collected in arrays $\boldsymbol{v}^n, \boldsymbol{i}^n$. The internal multiport $\mathcal{G}$ is defined by its admittance matrix

$$\begin{bmatrix} \boldsymbol{i}^p \\ \boldsymbol{i}^n \end{bmatrix} = \begin{bmatrix} \boldsymbol{G}_{pp} & \boldsymbol{G}_{pn} \\ \boldsymbol{G}_{np} & \boldsymbol{G}_{nn} \end{bmatrix} \begin{bmatrix} \boldsymbol{v}^p \\ \boldsymbol{v}^n \end{bmatrix} = \boldsymbol{G} \begin{bmatrix} \boldsymbol{v}^p \\ \boldsymbol{v}^n \end{bmatrix}. \tag{25}$$

The internal ports are closed on capacitive loads

$$\boldsymbol{i}^n = -\boldsymbol{C}_n \dot{\boldsymbol{v}}^n \tag{26}$$

where matrix $\boldsymbol{C}_n$ stores the capacitance values in its main diagonal with all other entries vanishing. Several representation choices are possible for the transfer matrix associated to $\mathcal{H}$, admittance, impedance, and scattering being the most typical. We concentrate on the latter, since actual frequency-domain VNA measurements lead naturally to scattering parameters. Therefore, we derive the input–output transfer matrix, using incident waves $\boldsymbol{a}^p$ and reflected waves $\boldsymbol{b}^p$ as independent and dependent variables, respectively. We use current normalization for these waves, with a common reference impedance $R_0 = 1/G_0$. Thus

$$\begin{aligned} \boldsymbol{a}^p &= \boldsymbol{G}_0 \boldsymbol{v}^p + \boldsymbol{i}^p \\ \boldsymbol{b}^p &= \boldsymbol{G}_0 \boldsymbol{v}^p - \boldsymbol{i}^p = \boldsymbol{a}^p - 2\boldsymbol{i}^p \end{aligned} \tag{27}$$

with $\boldsymbol{G}_0 = G_0 \boldsymbol{I}$. Combination of (25)–(27) leads to a state space representation of $\mathcal{H}$

$$\begin{cases} \dot{\boldsymbol{x}}(t) = \boldsymbol{A}\boldsymbol{x}(t) + \boldsymbol{B}\boldsymbol{a}^p(t) \\ \boldsymbol{b}^p(t) = \boldsymbol{C}\boldsymbol{x}(t) + \boldsymbol{D}\boldsymbol{a}^p(t) \end{cases} \tag{28}$$

where

$$\begin{aligned} \boldsymbol{A} &= -\boldsymbol{C}_n^{-1}\left[\boldsymbol{G}_{nn} - \boldsymbol{G}_{np}(\boldsymbol{G}_{nn} + \boldsymbol{G}_0)^{-1}\boldsymbol{G}_{pn}\right] \\ \boldsymbol{B} &= -\boldsymbol{C}_n^{-1}\boldsymbol{G}_{np}(\boldsymbol{G}_{nn} + \boldsymbol{G}_0)^{-1} \\ \boldsymbol{C} &= -2\boldsymbol{G}_0(\boldsymbol{G}_{nn} + \boldsymbol{G}_0)^{-1}\boldsymbol{G}_{pn} \\ \boldsymbol{D} &= 2\boldsymbol{G}_0(\boldsymbol{G}_{nn} + \boldsymbol{G}_0)^{-1} - 2\boldsymbol{I}. \end{aligned} \tag{29}$$

The frequency samples of the scattering matrix can be easily computed from the state space matrices as

$$\boldsymbol{S}(j\omega) = \boldsymbol{D} + \boldsymbol{C}(j\omega\boldsymbol{I} - \boldsymbol{A})^{-1}\boldsymbol{B}. \tag{30}$$

The above procedure ensures that the frequency responses generated via (30) are rational functions with N poles each. These poles are common among all transfer matrix entries. The bandwidth B encompassing all poles in the complex plane is inversely proportional to (and can be tuned by) the capacitance values in $\boldsymbol{C}_n$, which are assumed to be identical for simplicity. Thus, the proposed framework reduces the synthesis process to the generation of a suitable (constant) admittance matrix $\boldsymbol{G}$. This is constructed as

$$\boldsymbol{G} = \boldsymbol{P}\boldsymbol{G}'\boldsymbol{P}^{-1} + \boldsymbol{G}''. \tag{31}$$

Matrix $\boldsymbol{G}'$ is an almost-diagonal matrix having randomly generated complex eigenvalues $g_i = \mathrm{a}_i \pm j\mathrm{b}_i$ such that

$$\begin{aligned} a_i &= \Re\{g_i\} \in U([0, \vartheta G_{\max}]) \\ b_i &= \Im\{g_i\} \in U([-G_{\max}, G_{\max}]) \end{aligned} \tag{32}$$

where $G_{\max}$ is a suitable normalization constant and $U(\mathcal{I})$ denotes a random variable with uniform distribution within interval $\mathcal{I}$. The parameter $\vartheta \in [0, 1]$ represents a normalized loss factor, which allows to tune the amount of losses that will be present in the final responses (30). In particular, the closer is ϑ to zero, the more resonant will be the responses that will be lossless in the limit case $\vartheta = 0$. The closer is ϑ to one, the smoother will be the responses, with less evident resonance peaks. Matrix $\boldsymbol{G}'$ is constrained to be real by using 2×2 building blocks of the form

$$\begin{bmatrix} \mathrm{a}_i & \mathrm{b}_i \\ -\mathrm{b}_i & \mathrm{a}_i \end{bmatrix} \tag{33}$$

for each pair of complex conjugate poles. Matrix $\boldsymbol{P}$ in (31) indicates a nonorthogonal similarity transform built by iterative application of elementary transformations

$$\boldsymbol{P}_k = \begin{bmatrix} \cos\phi_{k1} & \cos\phi_{k2} \\ \sin\phi_{k1} & \sin\phi_{k2} \end{bmatrix} \tag{34}$$

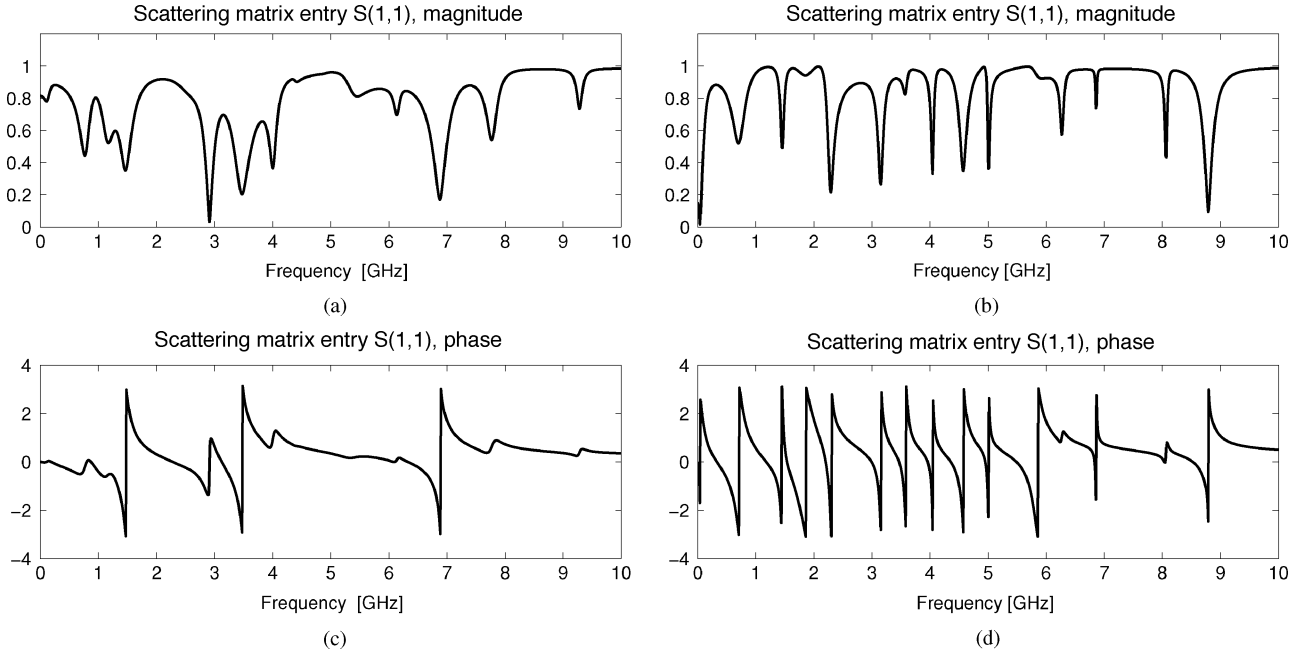

Fig. 15. Examples of synthetic scattering responses for a two-port structure (only S_{11} is shown) with two different loss factors. (a), (c) $\vartheta = 10^{-2}$ and (b), (d) $\vartheta = 10^{-4}$.

with $\phi_{k1} \neq \phi_{k2}$ to randomly selected pairs of rows/columns of $\boldsymbol{G}'$. This transform leads to the spread of the nonvanishing entries throughout the matrix so that coupling will be distributed evenly among all matrix elements. Finally, matrix $\boldsymbol{G}''$ is a skew-symmetric matrix with random upper-triangular entries

$$(G'')_{ij} \in U([-G_{\max}, G_{\max}]), \quad j > i \tag{35}$$

which provides additional shuffling of the coupling elements. As a byproduct, the above construction ensures that the multiport $\mathcal{G}$ is passive, since [2]

$$\boldsymbol{G} + \boldsymbol{G}^T \geq 0. \tag{36}$$

Consequently, the passivity of $\mathcal{H}$ is also guaranteed by construction.

To summarize, in addition to the number of poles N and ports P, there are four main parameters that allow to tune the scattering responses (30). The bandwidth B and the normalized loss factor ϑ lead approximately to the placement of the poles in a rectangular area of the complex plane with limits $(-\vartheta B, 0)$ along the real axis and $(-B, B)$ along the imaginary axis. The reference conductance for all ports is G_0. Finally, the degree of mismatch between the actual port impedance and the reference impedance is expressed by ratio $G_{\max}/G_0$. Some examples of generated responses for two different loss factors are shown in Fig. 15.

The above procedure allows the construction of various realizations of clean rational scattering responses. Noisy responses having a parameterized noise level (for testing the VF-AS algorithm under varying noise conditions) are now constructed. Given the scattering matrix (30) at given frequency samples ω_k, we build for each entry (i, j) the noisy response

$$\hat{S}_{ij}(j\omega_k) = S_{ij}(j\omega_k) + N_{ij}(\omega_k) \tag{37}$$

where $N_{ij}(\omega_k)$ represents a sequence of statistically independent and complex-valued random variables. Both real and imaginary parts are assumed to have a zero-mean Gaussian distribution with a variance that is parameterized by the SNR, defined as

$$\mathrm{SNR}_{\mathrm{dB}} = 10 \log_{10} \frac{\|S_{ij}\|^2}{\|N_{ij}\|^2} \tag{38}$$

and where the rms norm (10) is used. In all numerical experiments the SNR is kept constant for all transfer matrix entries in order to simplify the statistical analysis of the results. Examples of noisy responses with an SNR of 20 and 30 dB, respectively, have already been reported in Fig. 1.

ACKNOWLEDGMENT

The authors are grateful to C. Schuster of IBM for providing the measurements that were used for some of the test cases.

REFERENCES

[1] M. Nakhla and R. Achar, "Simulation of high-speed interconnects," *Proc. IEEE*, vol. 89, no. 5, pp. 693–728, May 2001.
[2] V. Belevitch, *Classical Network Theory*. San Francisco: Holden-Day, 1968.
[3] T. Kailath, *Linear Systems*. Englewood Cliffs, NJ: Prentice Hall, 1980.
[4] B. Gustavsen and A. Semlyen, "Rational approximation of frequency responses by vector fitting," *IEEE Trans. Power Del.*, vol. 14, no. 3, pp. 1052–1061, Jul. 1999.
[5] A. Semlyen and B. Gustavsen, "Vector fitting by pole relocation for the state equation approximation of nonrational transfer matrices," *Circuits Syst. Signal Process.*, vol. 19, no. 6, pp. 549–566, 2000.

[6] B. Gustavsen, "Computer code for rational approximation of frequency dependent admittance matrices," *IEEE Trans. Power Del.*, vol. 17, no. 4, pp. 1093–1098, Oct. 2002.
[7] B. Gustavsen and A. Semlyen, "A robust approach for system identification in the frequency domain," *IEEE Trans. Power Del.*, vol. 19, no. 3, pp. 1167–1173, Jul. 2004.
[8] S. Grivet-Talocia, Tutorial lecture on, "Characterization and macromodeling of 3D interconnects," presented at the 8th IEEE Workshop on Signal Propagation on Interconnects, Heidelberg, Germany, May 9–12, 2004.
[9] M. Abdel-Rahman, A. Semlyen, and M. R. Iravani, "Two-layer network equivalent for electromagnetic transients," *IEEE Trans. Power Del.*, vol. 18, no. 4, pp. 1328–1335, Oct. 2003.
[10] G. Antonini, "Equivalent network synthesis for via holes discontinuities," *IEEE Trans. Adv. Packag.*, vol. 25, no. 4, pp. 528–536, Nov. 2002.
[11] K. M. Coperich, J. Morsey, V. I. Okhmatovski, A. C. Cangellaris, and A. E. Ruehli, "Systematic development of transmission-line models for interconnects with frequency-dependent losses," *IEEE Trans. Microw. Theory Tech.*, vol. 49, no. 10, pp. 1677–1685, Oct. 2001.
[12] K. M. Coperich, J. Morsey, A. C. Cangellaris, and A. E. Ruehli, "Physically consistent transmission line models for high-speed interconnects in lossy dielectrics," *IEEE Trans. Adv. Packag.*, vol. 35, no. 2, pp. 129–135, May 2002.
[13] J. M. Griffith and M. Toupikov, "Time-domain modeling from S-parameters: Applicable to hard-disk drives," *IEEE Trans. Magn.*, vol. 39, no. 6, pp. 3581–3586, Nov. 2003.
[14] S. Grivet-Talocia, "Package macromodeling via time-domain vector fitting," *IEEE Microw. Wireless Comp. Lett.*, vol. 13, no. 11, pp. 472–474, Nov. 2003.
[15] S. Grivet-Talocia, H.-M. Huang, A. E. Ruehli, F. Canavero, and I. M. Elfadel, "Transient analysis of lossy transmission lines: An effective approach based on the method of characteristics," *IEEE Trans. Adv. Packag.*, vol. 27, no. 1, pp. 45–56, Feb. 2004.
[16] S. Grivet-Talocia, "Passive time-domain macromodeling of large complex interconnects," presented at the ACES04, 20th Ann. Rev. Progress Applied Computational Electromagnetics, Syracuse, NY, Apr. 19–23, 2004.
[17] ——, "The time-domain vector fitting algorithm for linear macromodeling," *Int. J. Electron. Commun.*, vol. 58, pp. 293–295, 2004.
[18] S. Grivet-Talocia, F. G. Canavero, I. S. Stievano, and I. A. Maio, "Circuit extraction via time-domain vector fitting," presented at the 2004 IEEE Symp. EMC, Santa Clara, CA, Aug. 9–13, 2004.
[19] S. Grivet-Talocia, I. S. Stievano, F. G. Canavero, and I. A. Maio, "A systematic procedure for the macromodeling of complex interconnects and packages," *Proc. EMC Europe 2004, Int. Symp. Electromagnetic Compatibility*, Eindhoven, The Netherlands, pp. 414–419, Sep. 6–10, 2004.
[20] B. Gustavsen and A. Semlyen, "Simulation of transmission line transients using vector fitting and modal decomposition," *IEEE Trans. Power Del.*, vol. 13, no. 2, pp. 605–614, Apr. 1998.
[21] ——, "Combined phase and modal domain calculation of transmission line transients based on vector fitting," *IEEE Trans. Power Del.*, vol. 13, no. 2, pp. 596–604, Apr. 1998.
[22] E.-P. Li, E.-X. Liu, L.-W. Li, and M.-S. Leong, "A coupled efficient and systematic full-wave time-domain macromodeling and circuit simulation method for signal integrity analysis of high-speed interconnects," *IEEE Trans. Adv. Packag.*, vol. 27, no. 1, pp. 213–223, Feb. 2004.
[23] E.-X. Liu, E.-P. Liu, and L.-W. Li, "Analysis of signal propagation on high-speed planar interconnect systems based on full-wave and macromodelling techniques," *Microw. Opt. Technol. Lett.*, vol. 39, no. 3, pp. 183–187, Nov. 2003.
[24] M. J. Manyahi and R. Thotappillil, "Transfer of lightning transients through distribution transformer circuits," in *Proc. Int. Conf. Lightning Protection 2002 (ICLP)*, Cracow, Poland, Sep. 2–6, 2002, pp. 435–440.
[25] V. I. Okhmatovski and A. C. Cangellaris, "Evaluation of layered media Green's functions via rational function fitting," *IEEE Microw. Compon. Lett.*, vol. 14, no. 1, pp. 22–24, Jan. 2004.
[26] M. S. Sarto, A. Scarlatti, and C. L. Holloway, "On the use of fitting models for the time-domain analysis of problems with frequency-dependent parameters," in *Proc. IEEE Int. Symp. EMC 2001*, Aug. 2001, pp. 588–593.
[27] G. Selli, M. Lai, S. Luan, J. L. Drewniak, R. E. Dubroff, J. Fan, J. L. Knighten, N. W. Smith, G. Antonini, A. Orlandi, B. Archambeault, and S. Connor, "Validation of equivalent circuits extracted from S-parameter data for eye-pattern evaluation," in *Proc. IEEE Int. Symp. EMC 2004*, vol. 2, Aug. 2004, pp. 666–671.
[28] W. Beyene and J. Schutt-Ainé, "Accurate frequency-domain modeling and efficient circuit simulation of high-speed packaging interconnects," *IEEE Trans. Microw. Theory Tech.*, vol. 45, no. 10, part 2, pp. 1941–1947, Oct. 1997.
[29] K. L. Choi and M. Swaminathan, "Development of model libraries for embedded passives using network synthesis," *IEEE Trans. Circuits Syst. II*, vol. 47, no. 4, pp. 249–260, Apr. 2000.
[30] M. Elzinga, K. Virga, L. Zhao, and J. L. Prince, "Pole-residue formulation for transient simulation of high-frequency interconnects using householder LS curve-fitting techniques," *IEEE Trans. Comp. Packag. Manufact. Technol.*, vol. 23, no. 2, pp. 142–147, Mar. 2000.
[31] M. Elzinga, K. Virga, and J. L. Prince, "Improve global rational approximation macromodeling algorithm for networks characterized by frequency-sampled data," *IEEE Trans. Microw. Theory Tech.*, vol. 48, no. 9, pp. 1461–1467, Sep. 2000.
[32] S. Grivet-Talocia, F. Canavero, I. Maio, and I. Stievano, "Reduced-order macromodeling of complex multiport interconnects," presented at the URSI General Assembly, Maastricht, Belgium, Aug. 19–23, 2002.
[33] J. Morsey and A. C. Cangellaris, "PRIME: Passive realization of interconnects models from measures data," in *Proc. IEEE 10th Topical Meeting Electr. Perf. Electron. Packag.*, 2001, pp. 47–50.
[34] C. P. Coelho, J. Phillips, and L. M. Silveira, "A convex programming approach for generating guaranteed passive approximations to tabulated frequency-data," *IEEE Trans. Computed-Aided Design Integr. Circuits Syst.*, vol. 23, no. 2, pp. 293–301, Feb. 2004.
[35] B. Gustavsen and A. Semlyen, "Enforcing passivity for admittance matrices approximated by rational functions," *IEEE Trans. Power Syst.*, vol. 16, no. 1, pp. 97–104, Feb. 2001.
[36] S. Grivet-Talocia, "Enforcing passivity of macromodels via spectral perturbation of Hamiltonian matrices," in *Proc. 7th IEEE Workshop Signal Propagation on Interconnects*, Siena, Italy, May 11–14, 2003, pp. 33–36.
[37] ——, "Passivity enforcement via perturbation of Hamiltonian matrices," *IEEE Trans. Circuits Syst. I*, vol. 51, no. 9, pp. 1755–1769, Sep. 2004.
[38] D. Saraswat, R. Achar, and M. Nakhla, "Enforcing passivity for rational function based macromodels of tabulated data," in *Proc. 12th IEEE Topical Meeting Electrical Performance of Electronic Packaging*, Princeton, NJ, Oct. 27–29, 2003, pp. 295–298.
[39] *CST Microwave Studio Manual, Version 4,* Computer Simulation Technology GmbH, Germany, 2003.

Stefano Grivet-Talocia (M'98) received the laurea and the Ph.D. degrees in electronic engineering from the Politechnic University of Turin, Turin, Italy.

From 1994 to 1996, he was at the NASA/Goddard Space Flight Center, Greenbelt, MD, where he worked on applications of fractal geometry and wavelet transform to the analysis and processing of geophysical time series. Currently, he is an Associate Professor of circuit theory with the Department of Electronics, Polytechnic of Turin. His current research interests include numerical modeling of interconnects, applications of wavelets to computational electromagnetics, and passive macromodeling of lumped and distributed structures. He is the author of more than 60 journal and conference papers.

Dr. Grivet-Talocia was the Associate Editor for the IEEE TRANSACTIONS ON ELECTROMAGNETIC COMPATIBILITY from 1999 to 2001.

Michelangelo Bandinu received the laurea degree in electronic engineering from the Politecnico di Torino, Torino, Italy, 2005. He is currently a research assistant with the EMC Group at Politecnico di Torino, Italy.

After graduation, he joined the IBM Deutschland Entwicklung GmbH, Boeblingen, Germany, where he has been working in the field of packaging development within the IBM Systems and Technology Group. He has been engaged in modeling and simulation of interconnect structures including actual and future chip carriers, multi- and single-chip modules, cards, boards, and connectors. He is currently a research assistant with the EMC Group at Politecnico di Torino.